Micropulse lidar observations of tropospheric aerosols over northeastern South Africa during the ARREX and SAFARI 2000 dry season experiments

James R. Campbell,[1] Ellsworth J. Welton,[2] James D. Spinhirne,[3] Qiang Ji,[1] Si-Chee Tsay,[3] Stuart J. Piketh,[4] Marguerite Barenbrug,[4] and Brent N. Holben[3]

Received 23 May 2002; revised 7 November 2002; accepted 30 January 2003; published 9 April 2003.

[1] During the Aerosol Recirculation and Rainfall Experiment (ARREX 1999) and Southern African Regional Science Initiative (SAFARI 2000) dry season experiments, a micropulse lidar (523 nm) instrument was operated at the Skukuza Airport in northeastern South Africa. The lidar was colocated with a diverse array of passive radiometric equipment. For SAFARI 2000, a daytime time series of layer mean aerosol optical properties, including layer mean extinction-to-backscatter ratios and vertical extinction cross-section profiles are derived from the synthesis of the lidar data and aerosol optical depths from available AERONET Sun photometer data. Combined with derived spectral Angstrom exponents, normalized broadband flux measurements, and calculated air mass back-trajectories, the temporal evolution of the surface aerosol layer optical properties is analyzed for climatological trends. For dense biomass smoke events the extinction-to-backscatter ratio is between 50 and 90 sr, and corresponding spectral Angstrom exponent values are between 1.50 and 2.00. Observations of an advecting smoke event during SAFARI 2000 are shown. The smoke was embedded within two distinct stratified thermodynamic layers causing the particulate mass to advect over the instrument array in an incoherent manner on the afternoon of 1 September 2000. Significant surface broadband flux forcing of over -50 W/m^2 was measured in this event. The evolution of the vertical aerosol extinction profile is profiled using the lidar data. Finally, observations of persistent elevated aerosol layers during ARREX 1999 are presented and discussed. Back-trajectory analyses combined with lidar and Sun photometer measurements indicate the likelihood for these aerosols being the result of long-range particulate transport from the southern and central South America. *INDEX TERMS:* 0305 Atmospheric Composition and Structure: Aerosols and particles (0345, 4801); 0345 Atmospheric Composition and Structure: Pollution—urban and regional (0305); 0360 Atmospheric Composition and Structure: Transmission and scattering of radiation; 0394 Atmospheric Composition and Structure: Instruments and techniques; *KEYWORDS:* lidar, aerosols, biomass burning, Sun photometry, lidar ratio, SAFARI 2000

Citation: Campbell, J. R., E. J. Welton, J. D. Spinhirne, Q. Ji, S.-C. Tsay, S. J. Piketh, M. Barenbrug, and B. N. Holben, Micropulse lidar observations of tropospheric aerosols over northeastern South Africa during the ARREX and SAFARI 2000 dry season experiments, *J. Geophys. Res.*, *108*(D13), 8497, doi:10.1029/2002JD002563, 2003.

1. Introduction

[2] The climatic impact of biogenic, pyrogenic and anthropogenic surface emissions across the southern African subcontinent (described here as the region south of the 15°S latitude) has been the focus of much recent field research. The area is marked by significant industrial and domestic sulfate and carbon release. A dense network of generator stations situated along the Highveld of northeastern South Africa, responsible for most electrical power to the region, and the predominance of biomass burning, both as a domestic fuel source and in the form of savannah fires, are the most notable contributors [*Piketh et al.*, 1999]. Beginning with the 1992 South African Regional Science Initiative (SAFARI) field campaign, and continuing through numerous projects, including the 1999 Aerosol Recirculation and Rainfall Experiment (ARREX) [*Terblanche et al.*, 2000] and SAFARI 2000, many diverse data sets have been collected in the region through coordinated surface, airborne and satellite remote sensing and in situ sampling. The goal of these efforts is the accurate characterization of regional aerosol evolution, transport and eventual deposition, and an improved understanding of the regional climatic and biological repercussions of its presence in the atmosphere [*Swap et al.*, 2002].

[1]Science Systems and Applications, Inc., Greenbelt, Maryland, USA.
[2]Goddard Earth Sciences and Technology Center, University of Maryland, Baltimore County, Maryland, USA.
[3]NASA Goddard Space Flight Center, Greenbelt, Maryland, USA.
[4]University of The Witwatersrand, Gauteng, South Africa.

Copyright 2003 by the American Geophysical Union.
0148-0227/03/2002JD002563$09.00

[3] This article discusses observations made through colocated active and passive remote sensing at the Skukuza Airport in the Krueger National Park of northeastern South Africa during the ARREX and SAFARI 2000 dry season components. A micropulse lidar (MPL), described by *Spinhirne* [1993], is the primary instrument of focus. Low-powered, eye-safe, and autonomously operated, the ruggedized MPL instrument is quite amenable to remote field operating conditions [*Spinhirne et al.*, 1995]. The MPL is a single-channel (523 nm), elastic backscatter lidar. Despite being low-powered, the MPL has been shown to be sensitive to nearly all forms of tropospheric cloud and aerosol [*Spinhirne*, 1993]. MPL instruments have been used in numerous recent aerosol-related field experiments including the Indian Ocean Experiment (INDOEX) [*Welton et al.*, 2002a], the Aerosol Characterization Experiment-2 (ACE-2) [*Welton et al.*, 2000; *Powell et al.*, 2000], ACE-Asia [*Welton et al.*, 2001a], and the Chesapeake Lighthouse and Aerosol Measurements for Satellites experiment (CLAMS) [*Smith et al.*, 2001].

[4] A single-channel lidar is somewhat limited in standalone capability, particularly in light of more robust lidar systems with depolarization and multiple channel capacities used during SAFARI 2000 [*McGill et al.*, 2003], and previous African field campaigns [e.g., *Fuelberg et al.*, 1996; *Browell et al.*, 1996]. The advantage of the MPL instrument is in its practicality (ease in remote deployment), and ability to make continuous full-time measurements. In addition to the lidar a diverse suite of passive radiometric instrumentation was operated simultaneously at the airport site. A CIMEL Sun photometer also operated less than two kilometers away in the Skukuza base camp. Integration of these data sets, as well as corollary information derived from upper air back-trajectories, reveals much information on the optical characteristics of the incident aerosols, and well as qualitative information on the nature of the aerosols being observed.

[5] In this presentation we examine the temporal evolution of local dry season aerosol optical parameters. Particular attention is given to the layer mean extinction-to-backscatter ratio (S), derived by combining lidar particulate backscatter and Sun photometer aerosol optical depth measurements. MPL instruments serve an ancillary purpose in collecting ground-validation data sets for the National Aeronautics and Space Administration (NASA) Earth Observing System (EOS) Geoscience Laser Altimeter System (GLAS) project. Proposed GLAS data processing algorithms specify a priori knowledge of this parameter [*Palm et al.*, 2001]. However, while numerous investigations have increased our understanding of this parameter with global consequence [e.g., *Takamura et al.*, 1994; *Anderson et al.*, 2000; *Peppler et al.*, 2000; *Welton et al.*, 2000; *Ansmann et al.*, 2000; *Ferrare et al.*, 2001; *Voss et al.*, 2001; *Welton et al.*, 2001a], and modeling studies have supplemented their work [e.g., *Ackermann*, 1998], practical characterization of the regional variation of S is still incomplete. The findings presented here, combined with similar measurements made by the cloud physics lidar [*McGill et al.*, 2003] aboard the NASA ER-2 aircraft [*King et al.*, 2003] will be used in this cause. Variation in S and spectral Angstrom exponent calculations, combined with analysis of upper air back-trajectories allow us to investigate distinct smoke and haze conditions observed during the SAFARI 2000 experiment relative to otherwise ordinary conditions.

[6] Two case studies are also examined. The first describes measurements of an evolving smoke plume from nearby biomass fires observed advecting over the instrument array. This case is unique as the smoke was observed to have evolved within separate boundaries of two vertically and thermodynamically distinct layers. Combined with surface flux measurements, this case is fully characterized with mind kept to the potential for validation of modeling studies on downwind smoke plumes [e.g., *Trentmann et al.*, 2002] and regional smoke transport. The second study describes the unexpected observation of persistent elevated aerosol layers (throughout the troposphere) during ARREX. The available evidence indicates a strong likelihood that they be the result of long-range transport of particles from a South American continental source via strong westerly upper level advection. The exact nature of the aerosols is unknown, though potential sources are discussed. The prolonged existence of significant elevated aerosol layers would prove bothersome to passive satellite algorithm retrievals that constrain observed aerosol characteristics to the surface layer. Additionally, long-range aerosol transport modeling studies require regional characterization of the vertical aerosol structure to interpret model output. With no previous evidence for intercontinental aerosol transport between South America and southern Africa, these observations are potentially very significant. Note that cross-validation studies involving Skukuza MPL data sets and measurements from airborne instrumentation during SAFARI 2000 can be found in papers by *Schmid et al.* [2003] and *McGill et al.* [2003].

2. Instrument Setup and Data Processing

[7] A common research site was used during both SAFARI 2000 and ARREX. The site encompassed the southwestern corner of the Skukuza Airport (24°59′S, 31°35′E, 315 m ASL) in the Krueger National Park. A passive radiometric instrument array was constructed in a field across from two aviation hangers. This suite of instruments included a multifilter rotating shadowband radiometer, scanning microwave radiometer, and multiple devices measuring broadband solar (diffuse and direct) and infrared radiation, as well as specific target wavelengths. The MPL was operated at the hangers, varying in placement slightly by year, approximately 100 m from the passive array. A permanent Aerosol Robotic Network (AERONET) CIMEL Sun photometer site [*Holben et al.*, 1998] was in operation less than 2 km from the airport in the Skukuza base camp.

[8] Following *Campbell et al.* [2002], the MPL instrument used during ARREX featured a V2.0 optical configuration. The instrument was housed in dual insulated containers, allowing for environmentally sheltered outdoor operation, placed between the hangers to limit direct solar heating. The containers were mated top (optical transceiver) and bottom (power supplies, computer and scalar unit), with collard ducts in between the two to allow for shared wiring and circulation. A broadband-coated, optically flat window was mounted along the top face of the upper box nearest to

the transceiver. Despite much effort, the design of these containers failed to properly regulate and stabilize the internal thermal operating environment. *Welton et al.* [2002a] discuss MPL data sets where the thermal stability of the instrument has been compromised, and the difficulties in processing them. Quantitative analysis of the ARREX data sets was severely limited as a result. The MPL used during SAFARI 2000 featured a V2.1 optical design. The instrument was operated inside the northernmost hanger. Though this shelter was not ideally sealed or insulated, many of the thermally induced difficulties experienced the previous season were overcome. A window mount was constructed on top of the hanger to accommodate an optical-quality transmitting window. A ceiling-mounted fan placed in the ceiling hatch limited window condensation.

[9] During both experiments, very little instrument downtime was experienced (>90% collection efficiencies). For ARREX, data were recorded at a 30 m vertical resolution setting. A lower setting (75 m) was used the following year for SAFARI 2000. Both data sets were recorded in sixty-second averaged profiles, and stored to local disk (roughly 150,000 pulse integrations corresponding to the 2500 Hz laser pulse rate). Instrument calibrations were accomplished using techniques outlined by *Campbell et al.* [2002]. The airport complex is situated on a significant butte. Unobstructed horizontal sightlines were available in most directions. Calibration of the instrument near-range overlap function (done using a horizontally homogenous target scattering layer) was relatively easy, and done frequently to insure data quality.

[10] Normalization of raw MPL data requires accounting for ambient background light, instrument-specific correction terms, and solving for the system calibration coefficient through the lidar equation. *Campbell et al.* [2002] discuss the algorithm and assorted techniques used to develop the raw data to the point of uncalibrated backscatter (termed normalized relative backscatter, or NRB). *Welton and Campbell* [2002] outline the methods for calculating uncertainties for this algorithm and each of the instrument correction terms. Furthermore, *Welton et al.* [2002] describe an algorithm for solving the absolute calibration coefficient (C), as well as indirectly derived optical parameters (i.e., backscatter and extinction cross-section profiles, optical depth profiles and layer mean extinction-to-backscatter ratios), including uncertainties for all terms. These algorithms and techniques are relied upon for this work.

[11] In our analyses, we use 30-min averages of NRB profiles centered on an independent measurement of the total column aerosol optical depth. Solving for C (briefly described below) relies on an estimate of column particulate transmission rates. For both experiments CIMEL Sun photometer data, available through the AERONET online database at http://aeronet.gsfc.nasa.gov, was used as the reference source. Measurements from this instrument were used with an uncertainty taken to be ±0.01 corresponding to their level 2.0 product [*Holben et al.*, 1998]. *Campbell et al.* [2000] describe the variability of C over a diurnal cycle using an MPL. To insure accurate data processing with the lowest quantifiable uncertainties, we restrict our analyses for this presentation to daytime periods where CIMEL measurements were available. Ambient background light decreases signal-to-noise rates significantly during the daytime, therefore requiring significant profile averaging for analysis.

[12] The algorithm described by *Welton et al.* [2000] employs a user-specified range above the surface aerosol layer, and free of particulate backscatter, from which to solve for C. After this calculation, the algorithm then searches for the top height of the aerosol layer in order to properly run a backward Fernald numerical inversion [*Fernald*, 1984] to solve the two unknowns in the lidar equation (particulate backscatter coefficient, and particulate transmission). The result is a layer mean value of S, and profiles of extinction and backscatter coefficients. In order to automate this algorithm, we document in Appendix A the basic approach to first solving for the top of the aerosol layer, so as to choose a range for solving for C as near to the instrument as possible. This has a significant effect on decreasing the uncertainty in C that, in turn, improves the uncertainty in those subsequently derived parameters dependent upon it.

3. SAFARI 2000 Optical Characteristics

[13] In this section we examine optical properties derived from combined lidar and Sun photometer data collected during SAFARI 2000. We supplement these findings with air mass back-trajectories calculated using the National Oceanic and Atmospheric Administration (NOAA) Hybrid Single-Particle Lagrangian Integrated Trajectory (HYSPLIT) Model to infer the nature of the aerosols investigated relative to local source regions and predominant flow. HYSPLIT model calculations can be interactively accessed via the NOAA Air Resources Laboratory Web site at http://www.arl.noaa.gov/ready/hysplit4.html. During SAFARI 2000, the MPL was operated from 18 August through 22 September. Low clouds spoiled much of the last week of this period, so we focus here on the period through 13 September inclusive. Corresponding to each day, three-day back-trajectories were calculated from 0000 UTC at five atmospheric levels (surface, 850, 700, 600 and 500 hPa). It was found that, in general, the surface to 850 hPa layers had similar transport patterns, while in the upper atmosphere circulation also correlated well, though different from that at the surface. We differentiate between the two layers in our discussion.

[14] Figure 1 is a collection of results encompassing the entire SAFARI 2000 period including: daily classifications of derived back-trajectories for the surface and upper layers (Figure 1a), algorithm output (S with error bars, and top of the surface aerosol layer, Figures 1b and 1e, respectively) and the spectral Angstrom exponent (AE, Figure 1c) and 523 nm aerosol optical depth (hereto forth referred to as simply AOD, while implicitly understood to be at the MPL wavelength, Figure 1d) derived from available CIMEL data. For the back-trajectories, the surface and upper level classifications were broken out into five and four regimes respectively. Surface cases were divided into easterly (1), recirculated (referring cases where the airmass originated over the continent, was blown off over nearby waters, and recirculated back to Skukuza, (2), westerly (3), northerly (4) and southerly (5). Upper level cases were divided into west-northwesterly (1), jet stream westerly (2), recirculated northerly (3), and recirculated easterly (4). AOD values were

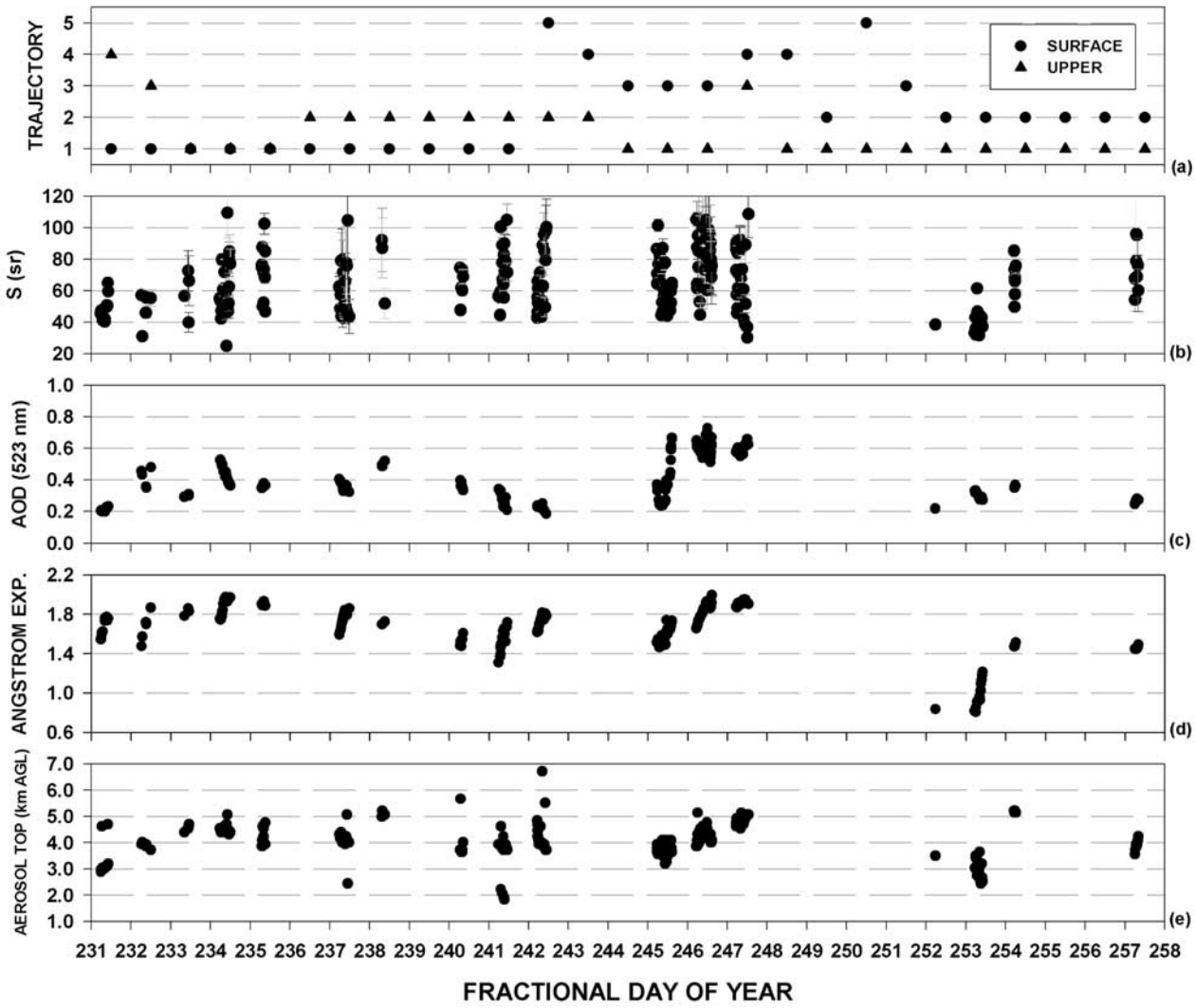

Figure 1. A summary of observations during the SAFARI 2000 experiment, 18 August to 13 September (fractional days 231 to 257 inclusive): back-trajectory classifications for lower (surface to 850 hPa) and upper levels (700 to 500 hPa), as described in the text (a), derived values of S for surface aerosol layer with uncertainty bars (b), AERONET CIMEL 523 nm aerosol optical depths (c), and Angstrom exponents (d), and the derived aerosol layer top height used to initiate algorithm inversion techniques (e).

derived using a second-order polynomial fit to the natural logarithm of AOD versus wavelength where at least four of the seven available CIMEL channels (between 340 and 1020 nm) reported data. AE values were similarly derived, though using a traditional power law curve-fit [e.g., *Angstrom*, 1964]. Owing to some fluctuations in MPL instrument thermal/optical stability, only those observations where the instrument temperature was less than 27.8 C are shown (chosen on the basis of prior experience with the subject instrument).

[15] As noted, derived values of S represent layer mean averages, as limited by the single-channel lidar instrument and Fernald inversion methodology. Algorithm noise, mostly due to cloud contamination of both the lidar profiles and ingested CIMEL AOD spectral profiles, is also expected to be present in our calculations. Error bars calculated for each case represent predominantly those quantifiable uncertainties arising through photon-counting statistics, both for the measured signal and for the instrument correction terms as referenced above. Therefore there is a floating uncertainty in our measurements that represents both the vertical inhomogeneity of S in the vertical column and algorithm noise for which we cannot account for. However, separate papers by *McGill et al.* [2003] and *Schmid et al.* [2003] show the MPL calculations (including profiles of extinction coefficient as well as S) to be in good overall agreement with other instruments running concurrently near or at Skukuza at various points during the experiment.

[16] Previous researchers have shown that the composition of the aerosol common to the region is highly complex, with many factors influencing it at any given time and place [e.g., *Piketh et al.*, 1999]. With regards to Figure 1, this seems acutely apparent. Stable synoptic conditions dominated the latter part of August, into early September allow-

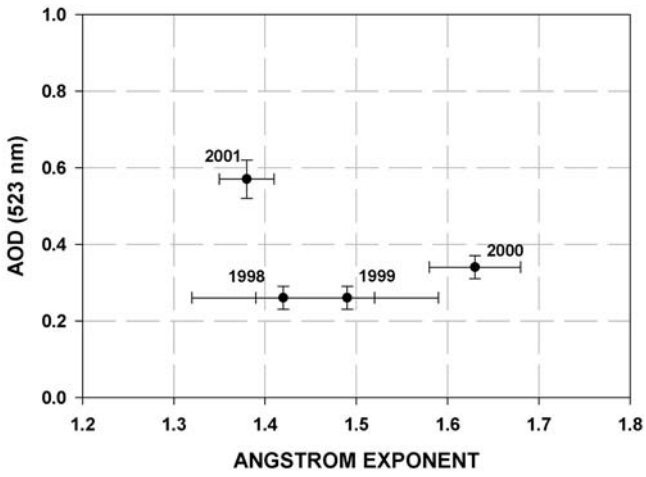

Figure 2. For the period 15 August through 15 September, the average aerosol optical depth versus average Angstrom exponent from available CIMEL Sun photometer data during 1998–2001 for the Skukuza Airport site.

ing for many data points. To establish some perspective, Figure 2 shows averages of AOD and spectral AE (with standard deviations) for the period 15 August through 15 September inclusive during the years 1998 to 2001, as derived from the AERONET database for Skukuza. With respect to AE, and to a lesser degree AOD, the 2000 season was somewhat unusual. Increases in both parameters from the previous two years indicates a downward shift in particle size distributions in local aerosols, and is consistent with an increase in overall particulate loading with respect to the prevalence of local biomass burning [*Reid et al.*, 1998; *Remer et al.*, 1996].

[17] From 18 to 22 August (fractional days 231–235) surface flow was consistently from the east, while upper level flow varied cyclically. Easterly surface flow represents onshore flow from the western Indian Ocean, leading to increased near-ground relative humidities. Aerosol humidification effects should be greatest in this pattern as convective mixing of the boundary layer enhances growth of particles each afternoon near the top of the lowest thermal inversion level [e.g., *Berg et al.*, 1998]. Since the observations reported here coincide mostly with synoptically stable, clear-sky conditions, thermal expansion and convective mixing of the boundary layer was likely simultaneously occurring. Evidence of resulting shift in particle size distribution can be seen in the diurnal increase of AE during each afternoon of the experiment (Figure 1d). The prevalence of regional biomass burning as a fuel source for cooking may also have had some influence, as local smoke concentrations regularly increased through the day. As AOD can be seen in Figure 1c to have decreased during most afternoons though, this effect was likely much smaller. The aerosol layer top height peaked near 5.00 km on 21 August (day 234), with corresponding peaks in AOD and AE. AE values approached and briefly exceeded 2.00, and were among the highest observed during the experiment. These measurements coincided with an upper level trajectory shift to west northwesterly. Such a pattern would increase the influence of continental transport from upwind biomass burning sources in Namibia, Botswana and Zambia. General trends in S calculations are in agreement with these observations. From 18 August, where upper level flow was easterly, then northerly, values were between 40 and 60 sr. Beginning on 20 August, when upper level trajectories became more westerly, much higher values, near and above 80 sr, were derived.

[18] Upper level trajectories from 23 to 28 August were westerly. This pattern decreased the influence of continental transport, increasing the impact of urban and industrial pollution sources from along the Highveld and in central South Africa. AOD values peaked on 25 August, though AE values did not reach the maximum values derived in previous west northwesterly upper level conditions (peaking near 1.90 on 24 August). Both parameters decreased notably through 28 August. S during this six-day period remained consistent with the previous smoke period, with values occurring between 40 and 80 sr. Relative variance in AE measurements here indicate some change in the aerosol composition, as hinted to by the change in upper level trajectories. However, relative persistence in S signifies that the overall absorptive character of the aerosols had not changed significantly.

[19] The three days, 1–3 September (days 245–247), were heavily influenced by smoke (to be examined further below). Beginning on 31 August, upper level trajectories shifted back to west northwesterly, where they would stay through the experiment (but for a slight deviation on 3 September). Nearer the surface, trajectories turned to westerly. The surface aerosol layer swelled to near 5.00 km, AE values peaked again near 2.0, AOD reached an experiment maximum over 0.70, and S remained between 40 and 80 sr. This period ended abruptly as a synoptic disturbance moved through the area inducing low and midlevel cloudiness for a number of days. Lower level trajectories varied between northerly (post-frontal) and westerly during this time. By 9 September (day 253) AOD values dropped to 0.20, and the aerosol layer top height was near 3.00 km. More notably, AE values plunged to near 1.00, and S values to roughly 40 sr. A more maritime-based aerosol composition was likely in place, as low-level trajectories were in a recirculating pattern.

[20] Figures 3a and 3b display the relative frequency of the individual air mass back-trajectories during the experiment for the upper and lower levels respectively. Trajectories at lower levels showed easterly and recirculated origin over 60% of the time. At upper levels, westerly and west northwesterly trajectories occurred nearly 90% of the time. In Figure 4a is a comparison of S to corresponding AE value for each of the data points shown in Figure 1. A similar comparison of AOD versus AE values is shown in Figure 4b. As discussed above, changes in AE showed appreciable correlation with back-trajectory shifts, and is therefore considered here to be a much more reliable indicator of changes to local aerosol composition. AE is directly related to the slope of a Junge-type size distribution. S is dependent upon the aerosol phase function and the single scatter albedo, and therefore is sensitive not only to changes in particle size, but also shape and refractive index. And, as aerosol species also have varying hydroscopic properties, particle size, shape, and refractive index are all dependent upon relative humidity to some degree. Given the

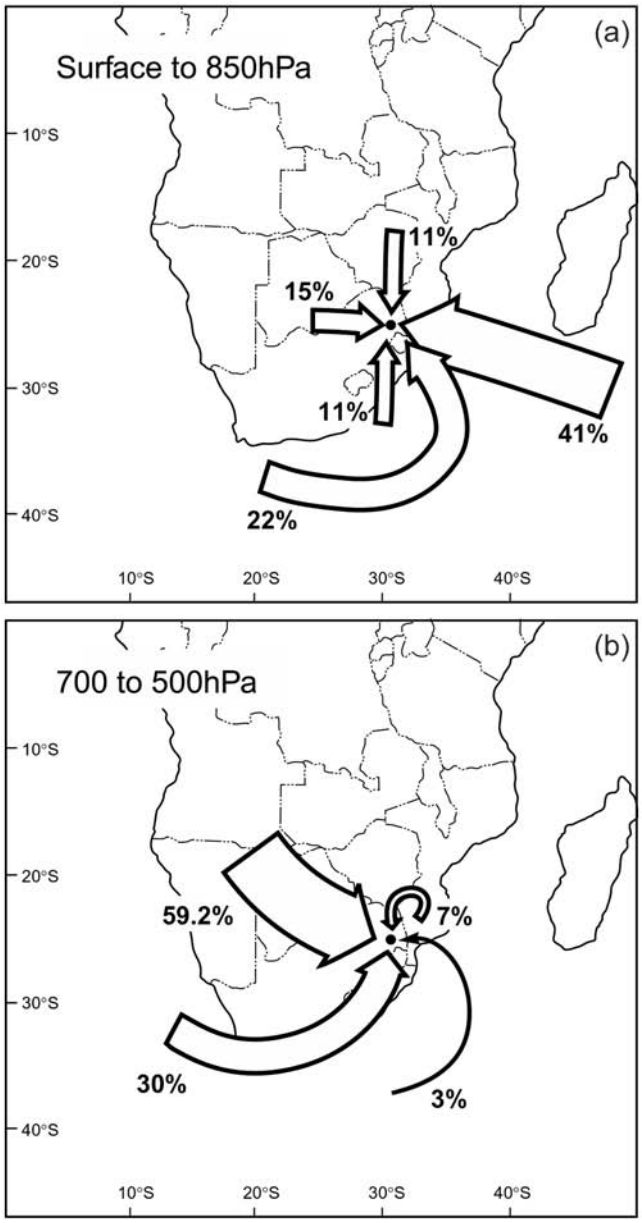

Figure 3. Corresponding to Figure 1, a breakdown of percentage frequencies of air mass back-trajectories for lower (a) and upper levels (b). From the surface to 850 hPa, trajectory classifications were broken into five categories: northerly, westerly, easterly, southerly and recirculated. From 700 to 500 hPa, trajectory classifications were broken into four categories: west-northwesterly, jet stream westerly, recirculated northerly, and recirculated easterly.

unique, yet chaotic regional mix of industrial and biomass pollutants, and the proximity of a major water source, overall variance in S should be quite high, and this is apparent in Figure 4a.

[21] Use of back-trajectory analyses allows the opportunity to better characterize the nature of the incident aerosols. Figures 5a–5d expand upon Figure 4a by breaking down the available data points into the four most commonly occurring lower/upper level trajectory scenarios: easterly/westerly (22%, Figure 5a), recirculated/west northwesterly (22%, Figure 5b), westerly/west northwesterly (15%, Figure 5c) and easterly/west northwesterly (11%, Figure 5d). The first of these scenarios (Figure 5a), was noted to have occurred between 23 and 28 August, and responsible for a greater influence of urban and industrial haze at upper levels. A linear regression calculation showed no apparent correlation, though AE values were otherwise between 1.30 and 1.90, and S varied between 50 and 90 sr. The second scenario (Figure 5b), occurring near the end of the experiment, produced the lowest number of data points in this breakdown. With recirculation prevalent at lower levels, a greater influence of maritime conditions on the aerosols yielded AE values between 0.80 and 1.60, while S varied between 30 and 70 sr. The most successful linear correlation coefficient was found in this scenario ($R = 0.79$). The third scenario (Figure 5c) coincided with the strong smoke event at the beginning of September. AE values were between 1.50 and 2.00, and S was between 50 and 90 sr. The second highest correlation coefficient was calculated in this scenario ($R = 0.31$). The final scenario (Figure 5b), responsible for the first significant biomass event at the beginning of the experiment yielded AE values between 1.70 and 2.00, and S values between 50 and 80 sr. This scenario correlates well with the biomass conditions noted in Figure 5b. As a whole, however, these findings suggest a low correlation between S and AE even when broken down by air mass origin. This suggests significant variability in the aerosol refractive index (S dependent upon through the single-scatter albedo term) as a function of particle size distribution (both dependent upon, S through the scattering phase function). If the former term were held constant, we would expect to see some sort of relationship otherwise. This again speaks to the overall complexity of the aerosols, despite air mass origin, at any given point in time.

[22] We briefly consider a less intensive analysis of the S results derived from this experiment. For aerosols, the absorption as quantified by the wavelength-dependent single scatter albedo is the major determining factor for a given AOD of the aerosol induced heating rate and surface shortwave flux forcing. Both S and the ratio of broadband shortwave diffuse to direct flux depend on aerosol absorption. For S, it is known that increasing the imaginary part of the refractive index, and thus absorption, leads to an increase in this parameter. This shows up most dramatically in Mie calculations for spherical particles. For a given size distribution and real part of the refractive index, S can change by an order of magnitude. In past studies [e.g., *Spinhirne et al.*, 1980] attempts have been made to estimate the imaginary part of the refractive index of aerosol from S measurements. Although there are large uncertainties introduced by particle nonsphericity, composition and unknown size distribution, results do fit a realistic model. Sky brightness is expected to decrease as aerosol absorption increases. A ''dark'' aerosol of lower single scattering albedo should lower the diffuse shortwave flux. Although there is also a scattering phase function effect, the primary impact of increasing the imaginary part of the refractive index in calculations is to lower the diffuse to direct ratio due to absorption. Surface albedo is also a major influence on the diffuse to direct ratio and must be known for a quantitative assessment. A higher surface albedo would magnify the aerosol absorption influence.

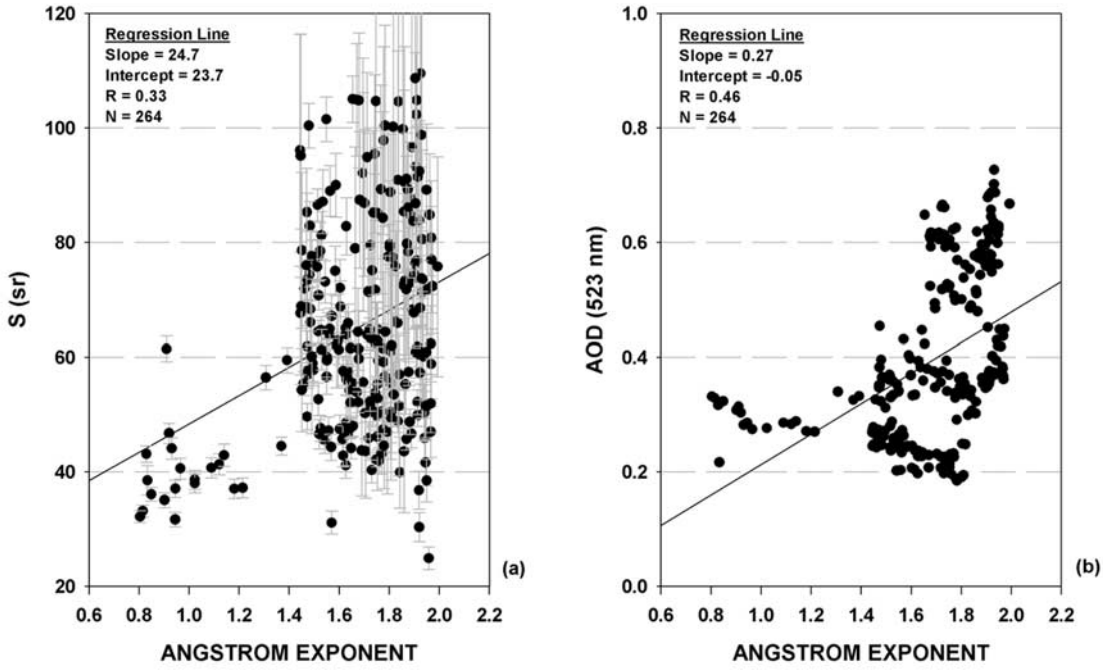

Figure 4. Corresponding to Figure 1, a comparison of Angstrom exponent values calculated from available AERONET CIMEL Sun photometer measurements vs. derived S values (a), and AERONET CIMEL 523 nm aerosol optical depths (b). Linear regression functions are shown, including relevant statistics such as the correlation coefficient.

[23] In Figure 6 is shown a comparison of normalized diffuse to direct shortwave flux ratio measurements versus the corresponding path normalized CIMEL AOD (multiplied by airmass) for three distinct grouping of S (less than 55, between 55 and 75 and greater than 75 sr). The expected dependence of a lower S with a higher diffuse to direct shortwave radiance ratio is clearly evident on the basis of linear regression fits to the available data points. High correlation coefficients were found with each fit. Linear functions were chosen on the basis of corresponding model calculations (not shown) using single-scatter albedo as the independent variable within these same axis parameters. For values of single-scatter albedo commonly associated with biomass burning aerosols (approx. 0.80) [e.g., *Reid et al.*, 1998], a roughly linear relationship was observed in the simulation results. Increasing nonlinearity was found with increasing divergence from these values. The data in Figure 6 are in agreement with the model, with variability in the derived slope values a reflection of the true nonlinearity of the relationship. As we have already concluded there to be significant complexity with respect to S, this agreement is likely tenuous (though still encouraging) given the effect of the scattering phase function over nearly thirty days of field observations.

4. Case Studies

[24] Two notable events were identified from the SAFARI 2000 and ARREX data sets, and are discussed in this section as case studies. First, we examine the evolution of a fresh smoke plume over the Skukuza site as observed by the surface instrument array. Second, observation of persistent elevated aerosols during ARREX led to an investigation into their potential nature and source. The lack of corroborating observations the following year makes these observations quite noteworthy.

4.1. Advecting Smoke Layer: 1 September 2000

[25] Our first case study deals with observations made on 1 September 2000 (fractional day 245), when smoke aerosols from recently begun fires upwind were observed advecting over the airport site. (Note that times are reported in this section in fractional day UTC. Local time at Skukuza was +0200 hours relative to UTC.) Figure 7 is a three-channel (0.66 μm, 0.55 μm, and 0.47 μm) early morning composite image of level 1B Moderate Resolution Infrared Spectrometer (MODIS) data taken aboard the NASA EOS Terra satellite (approximately 245.37). The Skukuza Airport (24.97°S, 31.58°E) is denoted in the image by a white dot. The satellite pass was centered well to the west of Skukuza (note the edge of the data swath on the right side of the image), so the resolution in the area of interest has been compromised to some degree. However, numerous fires and their resulting plumes existed in and around the vicinity of Skukuza. The highest concentration of fires was confined to a 3° by 3° grid directly north of the airport site. No fires were evident the previous morning in the available MODIS imagery.

[26] In Figure 8, MPL NRB data are displayed for the full day. The surface aerosol layer was confined to the first 4.00 km AGL. Two daytime balloonsonde profiles are shown in Figures 9a–9b. The top of the layer was capped by a slight temperature inversion near 580 hPa in the early morning (Figure 9a, 245.21) and near 560 hPa during the midafternoon (Figure 9b, 245.50). Measurements from a broadband solar radiometer at the airport are shown versus correspond-

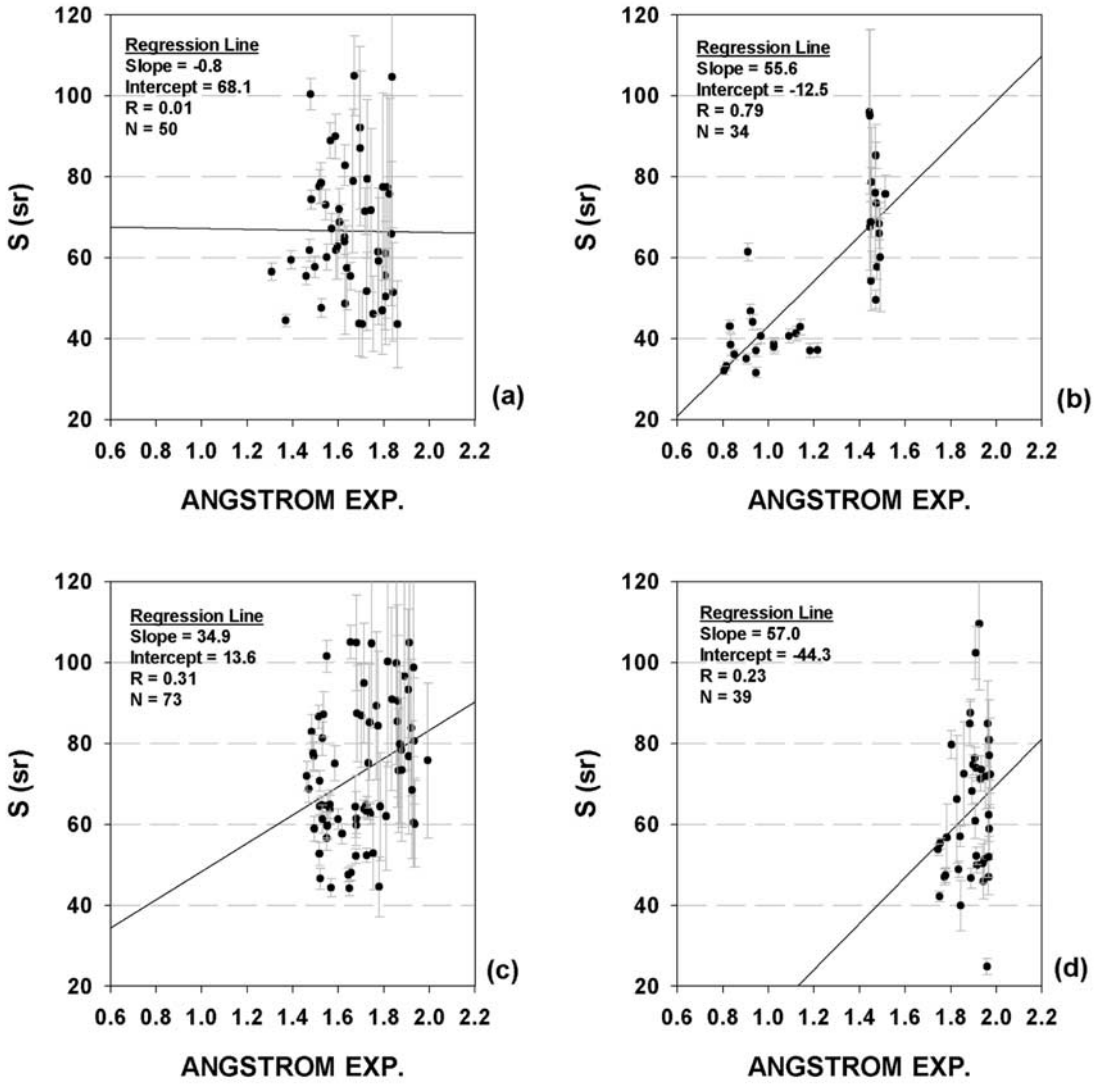

Figure 5. Corresponding to Figures 3 and 4, comparisons of Angstrom exponent values calculated from available AERONET CIMEL Sun photometer measurements vs. derived S values for the four most common lower/upper level back-trajectory classifications: easterly/westerly (a), recirculated/west-northwesterly (b), westerly/west-northwesterly (c), and easterly/west-northwesterly. Linear regression functions are shown for each figure, including relevant statistics such as the correlation coefficient.

ing "airmass" (defined as the inverse cosine of the solar zenith angle) in Figure 10. These data are broken into morning and afternoon observations, relative to the solar angle rising and lowering. Figure 11 is an expansion of Figure 1 for the subject day, with MPL algorithm output supplemented by corresponding CIMEL measurements. Finally, in Figures 12a–12c are three profiles of the extinction cross section as derived from the MPL measurements for the early morning (245.23), midafternoon (245.50), and late afternoon (245.60) respectively.

[27] What was unique about this event was that the advancing smoke plume, as witnessed at Skukuza, developed within two thermally separate layers. Aside from the upper inversion cap, a strong near-ground inversion was present in both radiosonde profiles (Figure 9). During the morning it was near 1.00 km. By afternoon, thermal expansion of the layer caused this boundary to lift to near 1.50 km. A clear delineation of the layers throughout the day is evident in both the NRB image (Figure 8), and the derived extinction profiles (Figures 12a–12c).

[28] From the NRB data, in the early hours of the day aerosols in the upper layer were well mixed. Some wisp-like structure (a sign of the oncoming event) was detected near 245.10. In the lower layer, a denser aerosol layer was detected. Though the first available sounding profile (Figure 9a) came a few hours later, it is likely that the extremely stable thermal structure measured in the lower layer at that time prevailed earlier as well. With the sunrise (near 245.20) an evolution of the layer to the more convectively unstable one seen in the afternoon (Figure 9b) commenced. This can be seen in the NRB data as the aerosol convectively mixed to near the inversion cap height with time (similar to as suggested for a humidified aerosol scenario in the previous section). Gradually this layer dis-

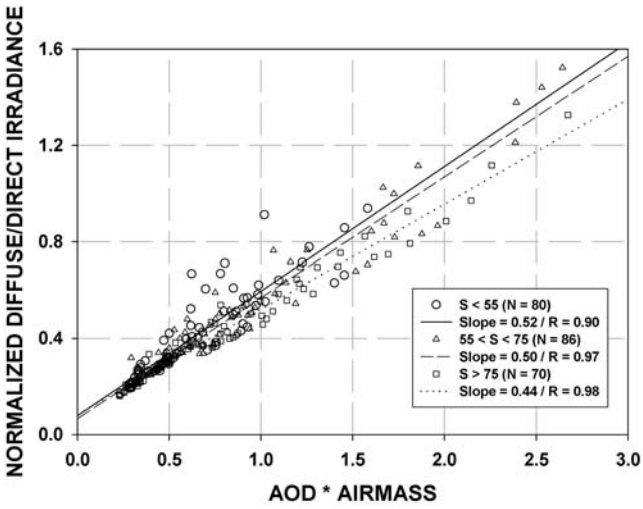

Figure 6. A comparison of the measured diffuse to direct broadband solar flux ratio versus path-normalized AERONET CIMEL 523 nm aerosol optical depth for three groups of S; less than 55 (plusses), between 55 and 75 (asterisks) and greater than 75 (open circles). Linear regression functions are shown, including relevant statistics such as the correlation coefficient.

sipated by 245.40. A snapshot of the evolving structure is seen in the first extinction profile (Figure 12a) where a peak value over 0.30 km^{-1} is seen in the lower layer, while the upper layer contained values under 0.10 km^{-1}. AE values beginning after sunrise (Figure 11) were near 1.50.

[29] By midafternoon (245.50), AE values increased, as did the AOD. The MODIS image, though earlier, showed that the corridor within the Lowveld was completely covered with varying degrees of smoke. However, dense concentrations were not yet at Skukuza. The NRB data at this time indicated that the smoke was almost exclusively confined to the upper layer. A peak extinction coefficient from the corresponding profile near 0.20 km^{-1} was detected at 2.50 km (Figure 12b). There was no indication yet of any significant increase in particulate matter (i.e., smoke) near the surface. This is presumably due to higher wind speeds above the near-ground inversion causing increased particulate advection in the upper layer (wind data was not available from the balloonsonde data).

[30] By late afternoon (245.60), smoke embedded in the lower layer reached the airport., and the AOD increased rapidly to near 0.70. The corresponding extinction profile (Figure 12c) shows the remarkable change in the structure of this layer. S, highly variable earlier in the day, converged at this time to near 60 sr. This observation is seemingly counter-intuitive given the high absorptive character of fresh smoke particles [e.g., *Reid et al.*, 1998; *Martins et al.*, 1998]. It signals a counter-balancing effect from the scattering phase-function term in S owing to an appreciable decrease in particle size distribution. (AE increased accordingly at this time to near 1.70). This event marked one of the densest smoke events with respect to AOD observed during the experiment.

[31] As discussed above, lower level back-trajectories were westerly and those in the upper level were west northwesterly. Stabilization in S at this time suggests that the vertical structure and composition of the aerosols was temporarily persistent. As such, it makes sense that the location of the upwind burning was in somewhat close proximity, as the MODIS imagery validates. Turbulent mixing over the lifetime of the plume had yet to have much effect in entraining dissimilar air, thereby inducing pockets of inhomogeneity, which would cause this parameter to fluctuate. The change in broadband forcing at the ground caused by the smoke was approximately -50 W/m^2, when compared to corresponding airmass values from earlier in the day (Figure 10). As smoke was observed in the upper layer during this earlier time, we estimate that the overall forcing of the smoke relative to the otherwise common background aerosol was actually somewhat higher than this amount.

[32] *Tyson et al.* [1995, 1996] and *Garstang et al.* [1996] discuss climatological air transport patterns over southern Africa in the lower troposphere, and corresponding aerosol recirculation in conjunction with the convective boundary layer. They also identify climatological trends in observed thermal inversion boundaries. Of note, *Tyson et al.* [1996] use downward looking lidar measurements made during SAFARI-92 to correlate aerosol concentrations with significant vertical thermodynamic structures. They found comparable discontinuities in aerosol concentration with each incident layer, though they did not document a case such as this.

[33] Transport-modeling efforts involving smoke in such a unique thermal environment face a daunting task. The available data limits us from deriving any potential optical disparities between the two layers. However, we can safely assume that as the case further unfolded with time, a continued delineation of the layers led to two uniquely modified aerosol types. What is clear is that a significant amount of smoke had reached the upper thermal layer, and that it was advecting quickly upstream from that trapped in the lower layer. Models will need accurate characterization of the efficiency at which a plume may punch through an initial inversion (i.e., buoyancy), not to mention proper initialization of the ambient thermal environment itself. Finally, the evolution of the aerosol composition would need to be accurately depicted in response to entrainment and modification.

4.2. Elevated Aerosols During ARREX

[34] Though the MPL data from ARREX were not suitable for thorough algorithm processing, our second case study involves a portion of these data that contrasted with results derived from the 2000 season. Shown in Figure 13a are MPL NRB data from 7 September 1999. Cloud and heavy aerosol loading was present during the first two-thirds of the day. By early evening the upper troposphere could be identified and much aerosol structure was evident. This day represents one of the more significant examples amidst a near two-week period (between 24 August and 9 September) where detectable aerosol was measured well above the common near-surface stable layers. No such cases of upper tropospheric aerosols could be found in the SAFARI 2000 data sets.

[35] It is not readily obvious what the aerosols consist of. Interpretation of the available lidar and passive data alone is

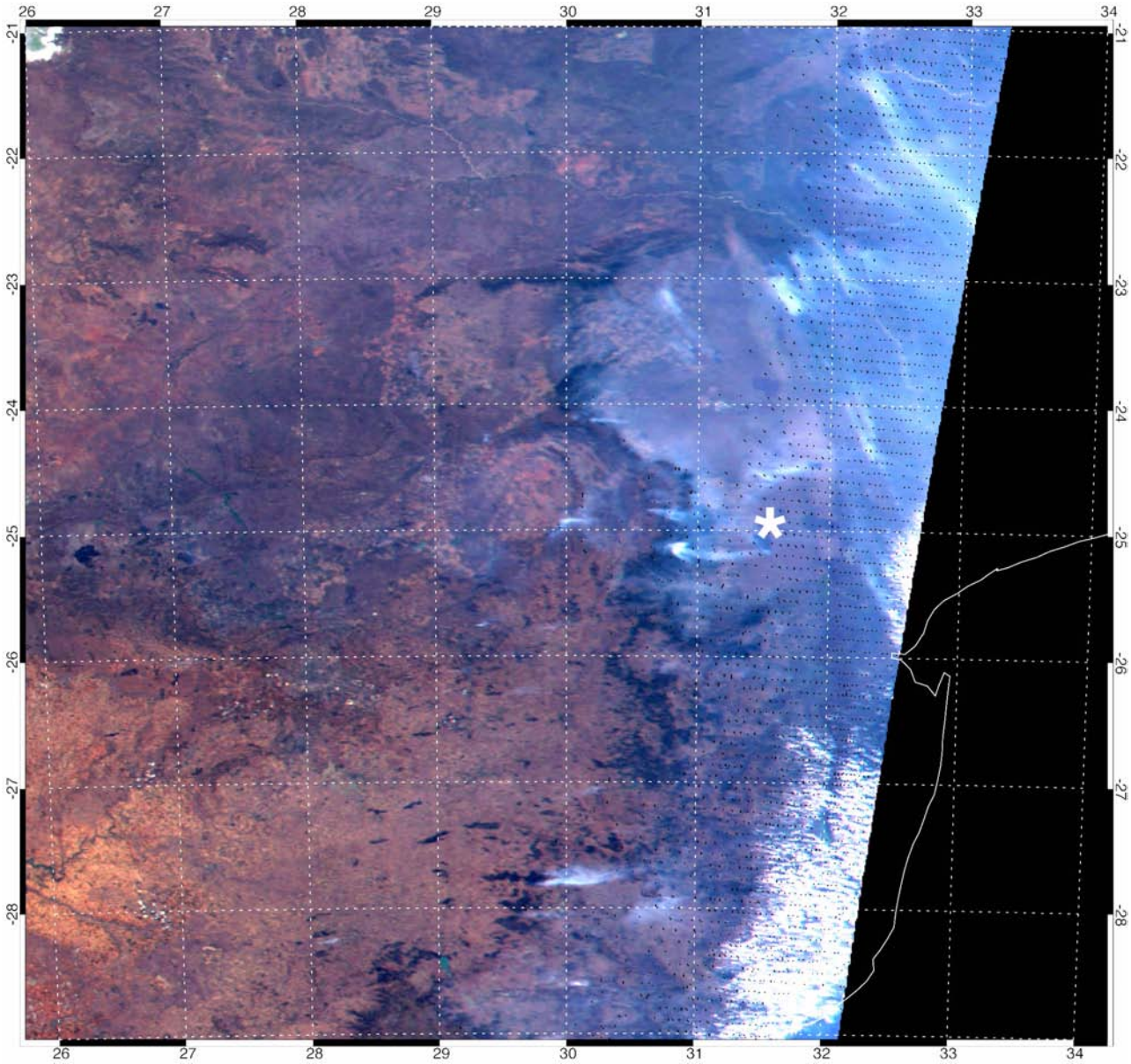

Figure 7. MODIS level 1B geolocated RGB composite imagery from bands 1, 4 and 3 (.66 μm, 0.55 μm, and 0.47 μm) for southeastern Africa from 0900 to 0905 UTC, 1 September 2000. Longitude/latitude designations are detailed along the border of the image, and the location of the Skukuza Airport site (24.97°S, 31.58°E) is labeled with a white star. The southeastern continental boundary is denoted on the right side of the image by a white border (though there are no data). An escarpment, separating the Highveld (west) and Lowveld (east) regions, can be identified as the darker winding terrain border beginning from the bottom of the figure near 28.00°E. Smoke plumes, and diffuse smoke aerosols are evident throughout most of the northern portion of the Lowveld. Hydrometeor clouds are evident in the southeastern sector, in close proximity to the Indian Ocean.

ambiguous. In situ aircraft measurements were made during the period, but the data were not conclusive. Ozone concentrations were found to be above normal background levels, which are indicative of biomass burn remnants. However, these flights were understandably coordinated to sample near-surface aerosols, and did not extensively penetrate the elevated layers. The possibility of downstream advection from fires in southern Zambia and neighboring areas exists [e.g., *Swap et al.*, 1996], though the lack of corroborating observations the following year raises significant uncertainty in this scenario.

[36] Though no sounding data were available from Skukuza for early September, the apparent structure in Figure 13a suggests particle stratification along thermal boundaries. This is consistent with a prolonged presence, whereby newly introduced particulate would likely show some degree of turbulent (mixing) structure. Seven-day air mass back-trajectories calculated for two upper tropospheric

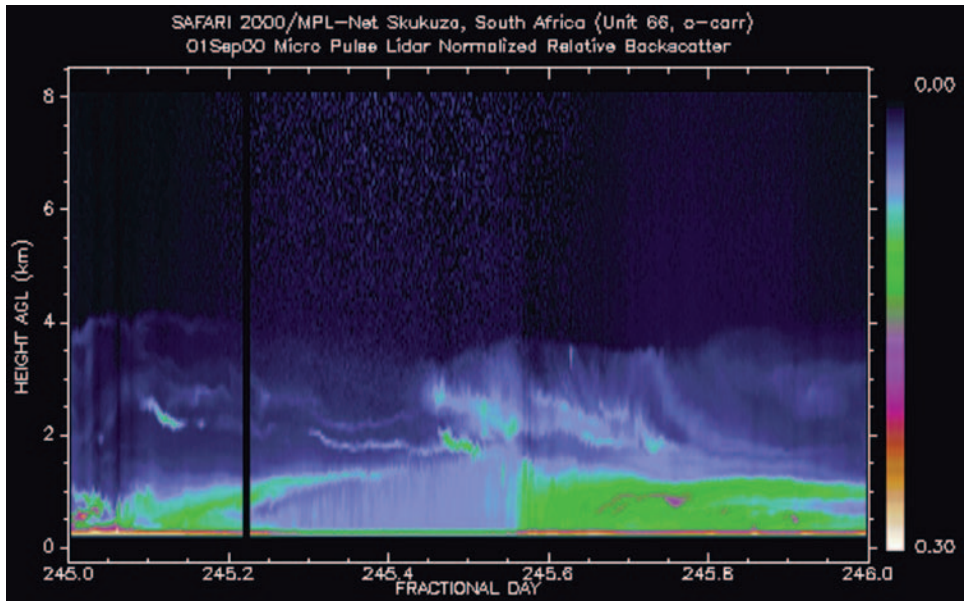

Figure 8. MPL normalized relative backscatter (counts*km^2/uj*us) data from 1 September 2000 at the Skukuza Airport site.

levels (6 km and 9 km) beginning from 0000 UTC 7 September at Skukuza are shown as Figure 13b. The trajectories show no air mass interaction with the southern African continent before reaching Skukuza, effectively eliminating the possibility of regional biomass influence. The origins of the air mass can be traced back from between days 3 and 5 to southern South America, where it appears these aerosols must have originated. Previous researchers have described aerosol transport events of South American biomass burning matter into the southern Atlantic basin [*Anderson et al.*, 1996; *Browell et al.*, 1996; *Kent et al.*, 1998]. Further advection to the African continent is plausible. Examination of AERONET CIMEL data from sites in central South America showed high AOD and AE values

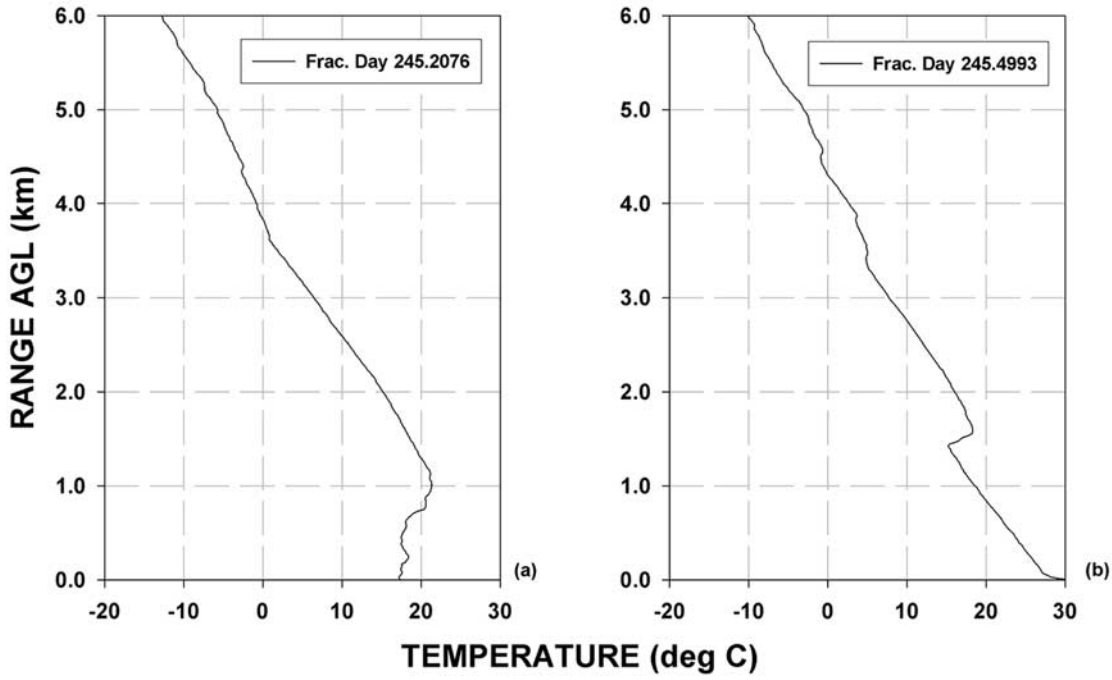

Figure 9. Balloonsonde profiles of temperature versus height above ground (km) from 1 September 2000 at approximately 0500 UTC (fractional day 245.2076) (a), and 1200 UTC (245.4993) (b) launched from the Skukuza Airport site.

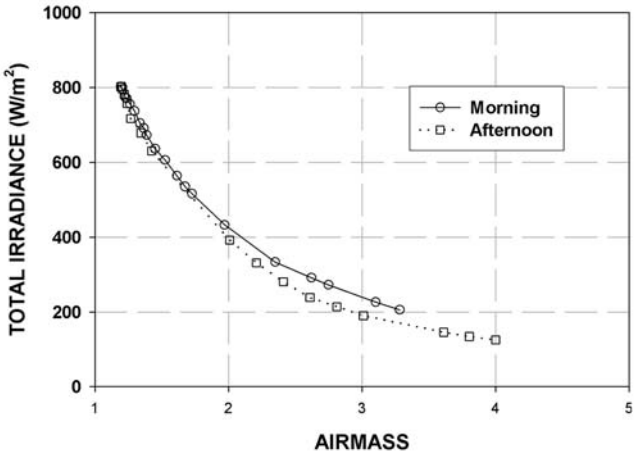

Figure 10. Broadband solar irradiance measurements versus airmass for 1 September 2000. Circles/solid represents measurements as Sun was rising, and square/dotted represents measurements as Sun was setting. Radiative forcing of afternoon smoke layer can be interpreted by comparing corresponding airmass measurements (i.e., early morning and late afternoon). The forcing of this event is estimated to be greater than -50 W/m^2.

from sites in western Brazil indicating an early start to the regional burning season. However, investigation of the available data from Skukuza (below) casts uncertainty on this seemingly reasonable scenario.

[37] This event was unique with regards to upper level transport. In Figures 14a and 14b respectively are seven-day air mass back-trajectories from 0000 UTC at Skukuza for the ARREX (sample cases only, 17 days) and SAFARI 2000 (entire study, 27 days) periods. An intermediate upper tropospheric starting level (7.50 km) was used. Transport trajectories during ARREX were more persistent, and displaced southward relative to those calculated for SAFARI 2000. Air mass encounters with the South American continent during ARREX were more common than SAFARI 2000 (85% to 75%). They nearly all occurred within 3–5 days before reaching Skukuza (not implicitly shown, though greater wind speeds can be inferred from Figures 14a and 14b), while between 30° and 35°S, compared to between 4 and 7 days and within 15° and 35°S the following year. The southward displacement of the ARREX trajectories is in disagreement with previous studies of South American biomass burning particulate transport patterns into the southern Atlantic basin [*Nobre et al.*, 1998]. However, they do suggest that the upper level environment was ideally conducive to a persistent transport event, whatever the source. Such persistence in the predominant flow over a significant timescale is likely anomalous, which raises the question as to the dynamic likelihood of any such intercontinental transport event occurring. Of course, this also depends on the ultimate nature of the event, and the efficiency at generating a significant amount of elevated particulate matter, which could be advected great distances under such ideal conditions. Perhaps more interesting to contemplate is just how far these aerosols ultimately traveled downstream beyond southern Africa.

[38] MPL optical algorithm retrievals from these data were limited, but offered some intriguing evidence. Successful retrievals from 7 September found that the contribution to total column AOD of the elevated layers amounted to no more than approximately 0.05 ± 0.03 at 523 nm (not shown). CIMEL optical depths from this day at the same wavelength were approximately 0.22. AE calculations from 17 August to 10 September 1999 are shown in Figure 15, along with the seasonal average values from 1999 and 2000, as derived in Figure 2. A sharp decrease in this parameter corresponds with 7 September, with values less than 1.30. Such low AE observations are not congruent with measurements during biomass burning events in 2000, although they do not deviate significantly. However, considering the lower contribution of the unknown aerosols to total column optical depth, relative to the common haze layers near the surface (approximately 25% on the subject day), lower AE values indicate a secondary influence on column scattering by larger particles that bias the parameter to the lower value. From Figure 14, the lowest AE values (0.8 and below) were observed on 25 August (MPL data not shown). Elevated aerosols on that day were observed to near 10 km above ground, and their contribution to column AOD was much higher (estimated near 50%). These data suggest that the elevated aerosols consisted of relatively large particles, which is again inconsistent with those found during biomass burning episodes. Particle growth over time, perhaps through cloud interaction [*O'Dowd et al.*, 1999] given the great distances from the original source region is conceivably possible. To result in AE values less than 1.0, however, would have required a considerable mean particle size evolution.

[39] Aside from biomass burning, two alternate mechanisms have been identified as possible sources for the aerosols. The first is based on the existence of two deserts in southern South America, the Atacama (along coastal Chile between 18° and 30°S) and Patagonia (between roughly 73°–64°W and 55°–40°S shared between Chile and Argentina). *Grousset et al.* [1992] and *Iriondo* [2000] previously found evidence for intercontinental transport of Patagonia dust matter to the Antarctic Peninsula. Current global dust transport modeling efforts, such as the Georgia Tech/Goddard Global Ozone Chemistry Aerosol Radiation and Transport (GOCART) model consider both of these deserts as source generating regions [*Ginoux et al.*, 2001]. Surface winds in the Patagonia region during the subject time are at a seasonal peak, coinciding with the influence of wintertime extratropical cyclones [*Lassig et al.*, 1999] (a literary search on reference to similar phenomena for the Atacama Desert found no corresponding studies). Though AE values taken at face value are not consistent with those of dust [e.g., *Tanre et al.*, 2001], our previous reasoning of a low bias in AE caused by scattering owing to larger particles in the elevated layers makes dust a plausible candidate.

[40] The second scenario involves a phreatic eruption cycle of the Guagua Pichincha volcano (0°10′S, 78°36′W) in Ecuador from June to September 1999 [*Legrand et al.*, 2002]. Multiple events were observed during this cycle, with the most significant occurring on 24 August. Matter was projected over 6 km above sea level during that eruption. Volcanic aerosol transport has been the focus of

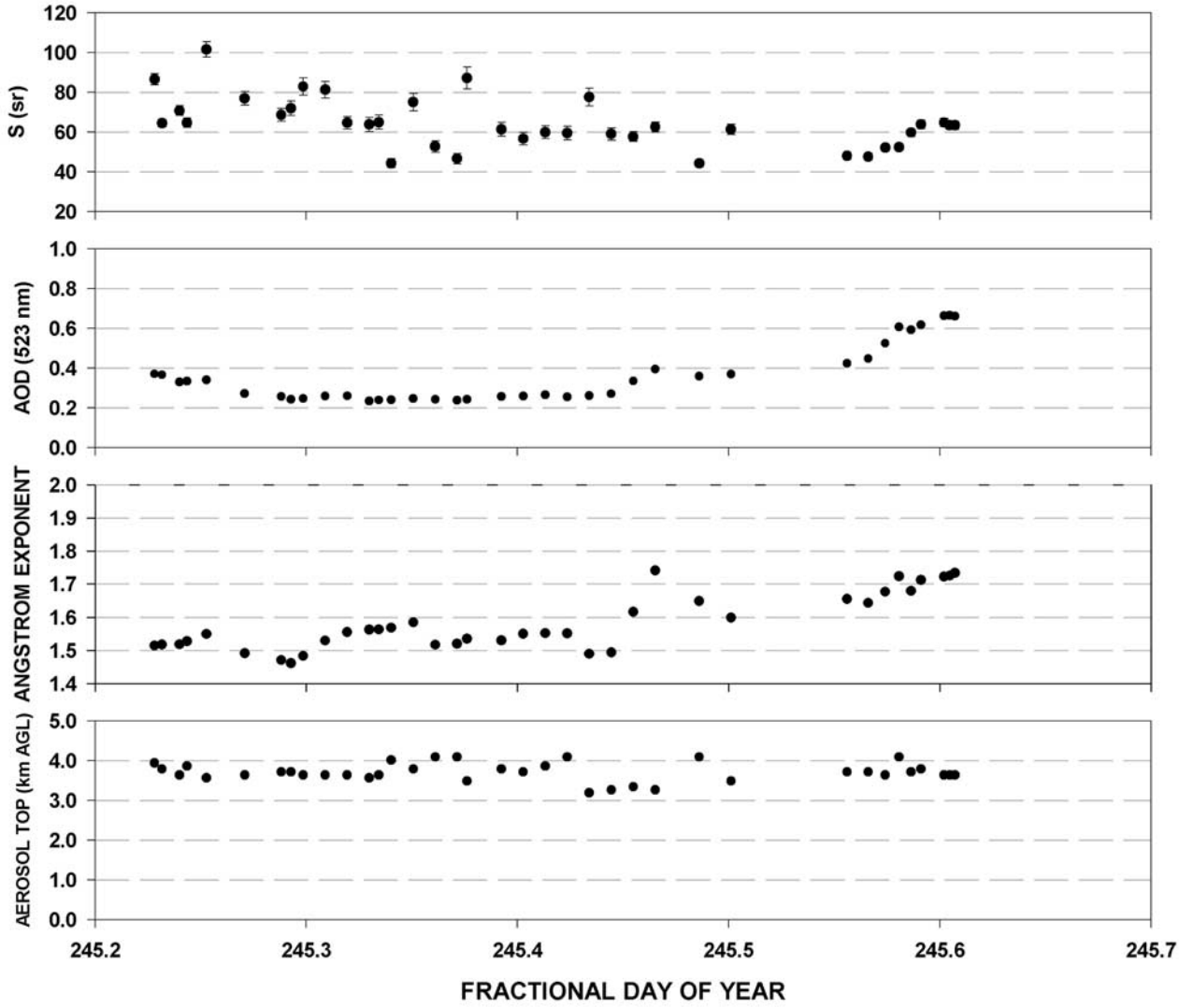

Figure 11. Corresponding to Figure 2 but expanded for 1 September 2000, without back-trajectory classification table.

much recent research as a consequence of the major Mt. Pinatubo eruption in June 1991. The optical characteristics of aerosols associated with that event, as well as other less significant eruptions, have been well documented [e.g., *Russell et al.*, 1996; *Schmid et al.*, 1997; *Watson and Oppenheimer*, 2001]. The proximity to the equator of this volcano, and subsequent lack of upper level steering flow at that latitude (so as to be entrained into the trajectories shown in Figure 14), and the large northerly displacement relative to the calculated trajectory tracks lessens the likelihood for this event being the responsible source. However, the timing and persistence of the eruptive activity, and the ability of volcanic particle intrusions to generate aerosol episodes significant on global scales are intriguing. Additionally, particle size distributions common to volcanic aerosols are larger with respect to biomass aerosols and could produce the observed AE bias previously noted.

[41] Though we cannot offer a definitive classification of the nature of these aerosols, we are at least very confident that their source was the South American continent. The striking contrast in vertical structure and temporal extent of these data to the more robust observations made the following year are at worst still noteworthy however. The statically stable nature of the southern African lower-troposphere should inhibit the prolonged protrusion of surface-elevated particulate matter well above the height of the uppermost inversion layers (~500 hPa). However, the extended presence of any particles, even with relatively low optical significance, would have some quantifiable effect on tropospheric column heating rates, thereby indirectly influencing the local meteorology and directly affecting surface radiative characteristics. As similar conditions were not witnessed during SAFARI 2000, those regional transport-modeling efforts, and radiative studies buoyed by data sets collected during that experiment should pay careful consideration to these findings. If by chance this scenario were actually a residual of local biomass burning, we can conclude on the basis of the case study discussed in the previous section that it would have required an extreme event to generate the significant buoyancies capable of

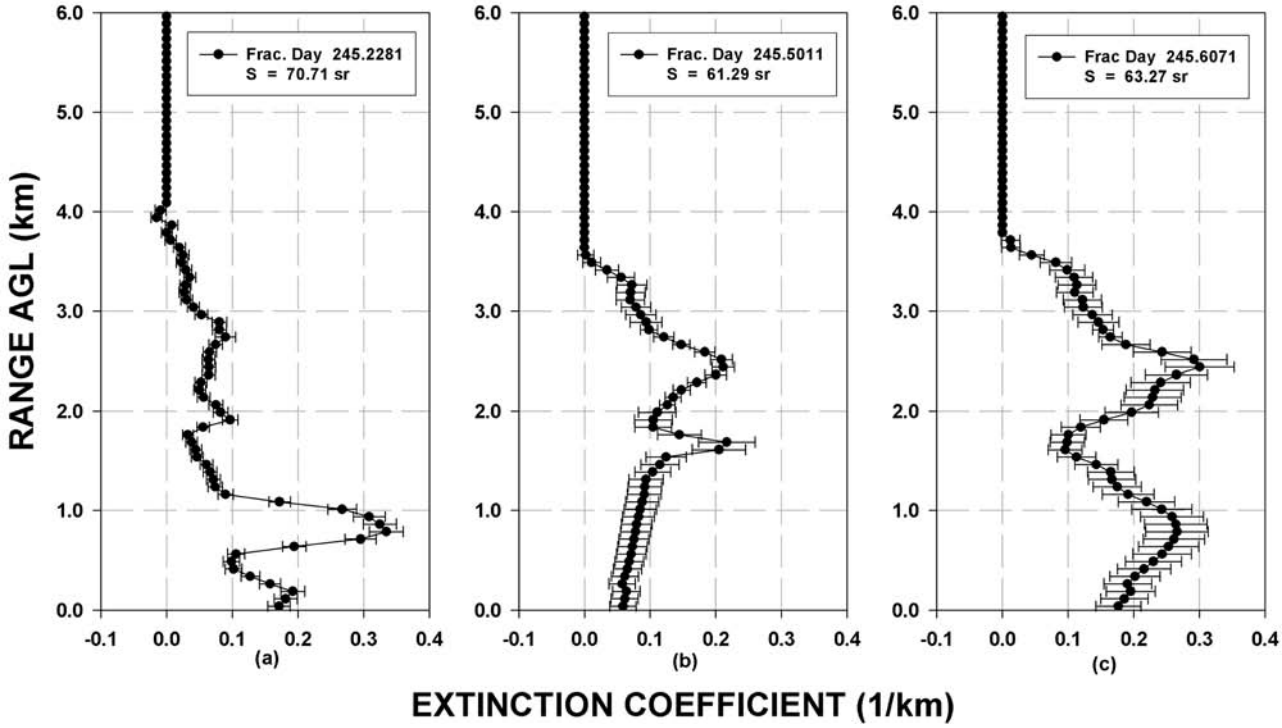

Figure 12. MPL-derived extinction cross-section profiles with uncertainty bars versus height above ground (km) for 30-min data periods on 1 September 2000; fractional day 245.2281 (a), 245.5011 (b) and 245.6071 (c). S for each case is noted.

penetrating the near-surface inversion layers over an extended period.

5. Conclusions

[42] In this paper we describe observations made during August and September for 1999 and 2000 at the Skukuza Airport in northeastern South Africa in concurrence with the ARREX and SAFARI 2000 field campaigns. The primary instrument of focus is a micropulse lidar instrument (MPL) supplemented with observations from colocated passive radiometric equipment and derived air mass back-trajectories. The purpose of these measurements is to enhance our understanding of the optical properties of regional aerosols, which are heavily influenced by industrial sulfate emissions and biomass burning. Specifically, regional characterization of the extinction-to-backscatter ratio (S) is of particular importance to satellite-based lidar programs as calibration reference points. We have shown that during the dry season months, there is great variability in this parameter as a function of air mass origin.

[43] Under dense smoke/haze conditions, S was found to vary between 50 and 90 sr. In west northwesterly upper level flow, which increases the influence of continental transport from prevalent upwind biomass burning locales, the spectral Angstrom exponent (AE) was found to be between 1.60 and 2.00. As air mass origins shifted at upper levels to more westerly, thereby inducing greater advection of urban and industrial pollutants, AE was found to reach a maximum only approaching 1.90 with common values much being much lower. In conditions affected by the influence of maritime aerosol modification and recirculation, S values dropped to between 40 and 70 sr, while AE values were between 0.80 and 1.60 in agreement with previous work [e.g., *Welton et al.*, 2000; *Voss et al.*, 2001]. The chaotic nature of the regional aerosol, based on air mass origin, and the inherently sensitive nature of the S owing to dependencies on various aerosol parameters make this value difficult to simply distinguish within the bounds of proposed seasonal look-up tables established to initiate satellite-based single-channel lidar aerosol property retrievals. AE values correlated much more clearly with changes in air mass origin in this study.

[44] Two case studies are detailed. The first describes the onset (morning/afternoon of 1 September 2000) of advecting smoke from nearby fires observed by the lidar and passive instrument array within the separate bounds of two vertically distinct thermal layers. We show the evolution of this event both in vertical profiles of particulate extinction cross section, S, and with respect to surface broadband flux and Sun photometer measurements. Significant surface shortwave forcing at the surface, greater than -50 W/m^2, was measured in this event. 523 nm aerosol optical depths exceeded 0.70 and AE values approached 1.80. The stable nature of the southern African lower troposphere and the prominence of multiple thermal inversion layers make these observations unique in the scope of global smoke/particulate transport. Additionally the efficiency at which rising smoke plumes are able to penetrate successive regional inversion layers, if and where present, will have a direct effect on local vertical heating rate profiles and surface flux rates. In this case, MPL observations show that the peak extinction cross sections in each layer were both roughly 0.30 km^{-1}. It can be concluded that a significant amount of the smoke matter reached the upper layer in this case.

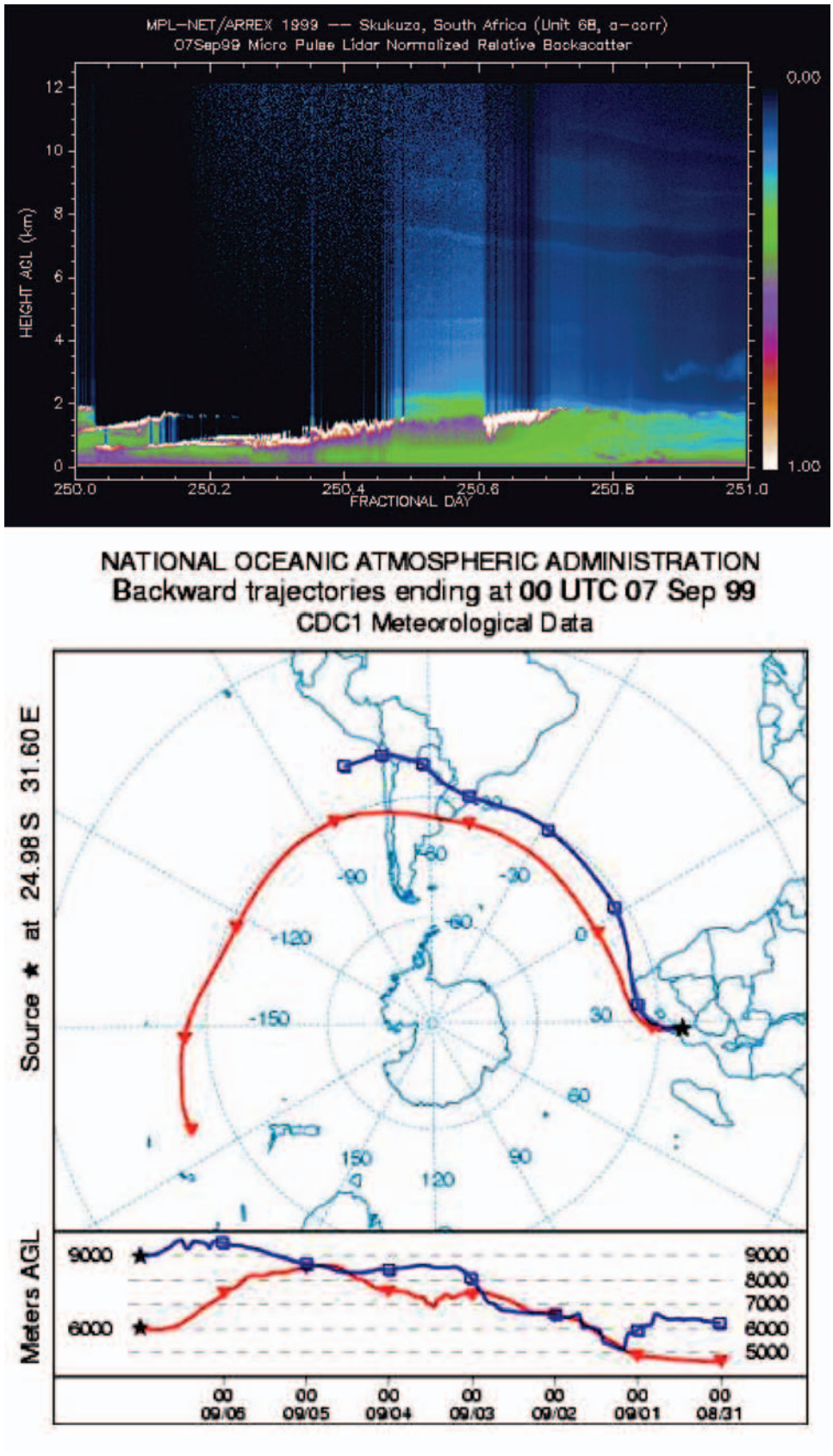

Figure 13. MPL normalized relative backscatter (counts*km^2/uj*us) from 7 September 1999 at the Skukuza Airport site (top), and seven-day NOAA HYSPLIT back-trajectory calculations for 6.00 and 9.00 km beginning at 0000 UTC from Skukuza (bottom).

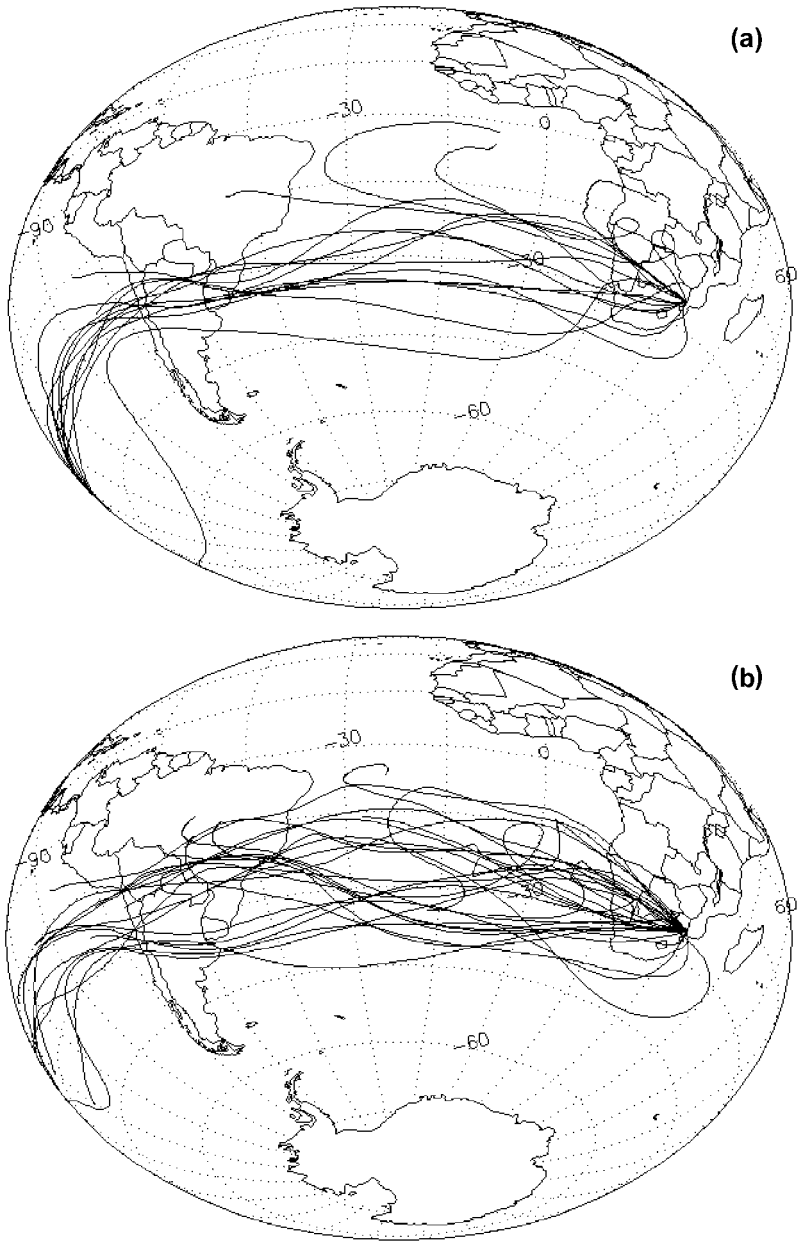

Figure 14. Seven-day air mass back-trajectories from 0000 UTC at 7.50 km from Skukuza for ARREX (24 August to 9 September 1999) (a) and SAFARI 2000 (18 August to 13 September 2000) (b).

[45] Finally, we present MPL observations of persistent elevated aerosols during ARREX. Analysis of daily seven-day back-trajectories from the period indicates that they likely were the result of intercontinental transport between southern South America and southern Africa. While previous researchers have shown the existence of biomass burning aerosols advecting from central South America into the southern Atlantic Ocean basin, ancillary passive measurements made at Skukuza are not in agreement with such a scenario being responsible. Two alternate hypotheses are presented: dust transport from the Patagonia and/or Atacama Deserts desert areas of southern South America, or elevated matter from the Guagua Pichincha volcano in Ecuador. The latter experienced significant eruptive activity from June to September 1999. These observations are unique in that upper tropospheric aerosols were not observed the following year during SAFARI 2000. Comparison with similar seven-day back-trajectories during the 2000 experiment showed anomalies in air mass interaction both in latitudinal displacement and length of day from Skukuza. Upper level winds were found to be more favorable for a sustained particulate transport event in ARREX than during SAFARI 2000. Should it be proven in subsequent analyses that these aerosols were the result of dust transport, previous observations of intercontinental transport from these deserts exists only to the Antarctic Peninsula [e.g., *Grousset et al.*, 1992; *Iriondo*, 2000]. Our findings, though ultimately not wholly conclusive, are potentially very noteworthy. Optical depth profiles derived using the lidar and Sun photometer data from the most significant

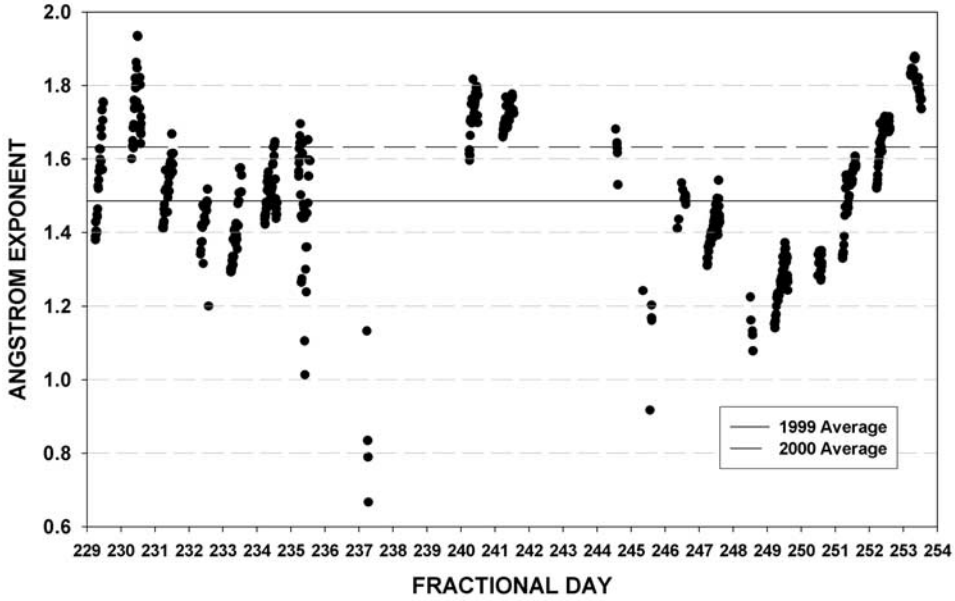

Figure 15. Angstrom exponent calculations from available AERONET CIMEL Sun photometer data for the period 17 August to 10 September 1999. Overlaid in the image are seasonal mean values for 1999 (solid) and 2000 (dashed) as described in Figure 2. 7 September 1999, as referenced in the text, corresponds to fractional day 250.

periods of the event show that the elevated aerosols contributed approximately 0.05 ± 0.03 at 523 nm, which is significant with regards to affecting column heating rates.

[46] Deployment of the MPL instruments for these experiments was coordinated through the recently formed NASA Earth Observing System (EOS) Micropulse Lidar Network project (MPLNET) [*Welton et al.*, 2001b]. The MPL-Net program was designed to establish a global network of MPL systems of long-term climatological cloud and aerosol research. In the coming years, instruments will be deployed at preexisting AERONET field sites to supplement colocated Sun photometer measurements with profiles of vertical structure. Additionally, field campaigns will be supported as deemed relevant. Data sets described in this paper are available online, and potential users are encouraged to visit the project website to make specific inquiries. The MPL-Net World Wide Web site can be accessed at http://mplnet.gsfc.nasa.gov/.

Appendix A

[47] In this section we describe an automated algorithm used to find the top of the surface aerosol layer from an individual (as stored operationally) or group-averaged MPL profile. When analyzing a single profile, or including it in a group average, a simple signal threshold filter is applied to every profile to avoid cloud contamination (D. D. Turner, personal communication, 1998). The search begins by finding the first range bin from the instrument where the ratio of NRB signal to NRB signal uncertainty is less than 2.00. Roughly speaking, this relationship is signal-to-noise ratio (SNR). However, SNR typically applies to the similar ratio but for raw signal. Given that there are instrument correction terms and related uncertainties mixed into this new value it would be inappropriate to title it as such. However, the general correlation is still valid. This corresponding range is considered the top of the resolvable vertical column (i.e., the range to which there is reliable signal in the profile). As a value of 1.00 indicates the point of absolute uncertainty with regards to interpreting a single bin, a value of 2.00 is used to make the interpretation stringent.

[48] For all range bins from the instrument to the "noise bin" a value for C is solved for using the derived AOD (to solve the two-way particle transmission path), and a modeled molecular scattering profile (as described by *Welton et al.* [2002]). Next, the resolution of the profile is degraded to 150 m and C is recalculated for each bin (with lower uncertainty due to averaging) up to the "noise bin." Clearly this methodology is flawed, as C will not be correct/applicable for every bin. However assuming that the entire aerosol layer is contained within a finite range in the area from the ground to the "noise bin," C will converge to a correct solution with range. In other words, C will be biased artificially high within the aerosol layer, but for the range past it, where backscatter is almost entirely molecular, the calculation will be accurate. Therefore we use the minimum value found in the degraded resolution profile (lower uncertainty) and use it as a base from which to normalize the individual bin values, such that

$$\chi(r) = C(r)/C^*(r^*) \tag{A1}$$

where C(r) is the C calculated at normal resolution, and C*(r*) is the base normalization value at the lower resolution (r*). The uncertainty of this relationship is given by

$$\partial\chi(r) = \chi(r)\text{*SQRT}\big((\partial C(r)/C(r))\text{\^{}}2 + (\partial C^*(r^*)/C^*(r^*))\text{\^{}}2\big) \tag{A2}$$

In a noise-free environment, the first bin from the ground to the "noise bin" where χ is equal to 1 could be considered free of aerosol and entirely composed of molecular components. However, in considering equation (2) we are restrained by the uncertainty of the signal and instead use the first bin where

$$\chi(r) < 1 + \partial\chi(r) \tag{A3}$$

to be the top of the aerosol layer. A 1.1 km range of bins beginning 300 m above the top of the aerosol layer (to offset small errors in the layer top search) is then designated as the calibration zone for solving C [*Welton and Campbell*, 2002].

[49] This somewhat simple technique does not differentiate between individual aerosol layers, rather it finds the top of the highest aerosol layer as determined by the first range bin containing signal derived from only molecular-scattering, as constrained by uncertainty. Two scenarios can occur which undermine the methodology. First, if separate elevated layers are present above the surface layer, such that a well-defined "clear slot" is evident in the signal profile, the algorithm will not search for their presence. Instead, it will solve for C assuming that the CIMEL AOD measurement was due entirely to transmission in the surface layer. Second, if the "noise bin" were to be found before reaching the top of the surface layer (e.g., dense haze), the algorithm would default to that point as representing the top of the layer. If this range were not within 300 m of being accurate, the algorithm would incorrectly choose the calibration zone. Both of these circumstances produce clearly erroneous values of C that are easily filtered out.

[50] **Acknowledgments.** The National Aeronautics and Space Administration (NASA) Earth Observing System program, and the NASA Sensor Intercomparison and Merger fund for Biological and Interdisciplinary Oceanic Studies support MPL research at the Goddard Space Flight Center. The authors wish to thank Dennis L. Hlavka, William D. Hart, Matthew McGill, Timothy D. Berkoff, and V. Stan Scott (NASA GSFC) for helpful insights and dedicated work on the MPL program, and Kristy Ross and Christoph Bollig (U. of Witwatersrand) for their assistance with the instruments in the field. We also thank Mark Gray (NASA GSFC) of the MODIS Atmosphere Team, who provided the composite image from 1 September 2000, and Lisa Harold (NASA GSFC), Wendy Job (Department of Geography, Archaeology and Environmental Studies, Wits University), and the Cougar Forum for their various forms of technical assistance. We gratefully acknowledge the comments of two anonymous reviewers, which significantly enhanced the original draft of this manuscript.

References

Ackermann, J., The extinction-to-backscatter ratio of tropospheric aerosol: A numerical study, *J. Atmos. Oceanic Technol.*, *15*, 1043–1050, 1998.

Anderson, B. E., et al., Aerosols from biomass burning over the tropical South Atlantic region: Distributions and impacts, *J. Geophys. Res.*, *101*, 24,117–24,137, 1996.

Anderson, T. L., S. J. Masonis, D. S. Covert, R. J. Charlson, and M. J. Rood, In situ measurement of the aerosol extinction-to-backscatter ratio at a polluted continental site, *J. Geophys. Res.*, *105*, 26,907–26,915, 2000.

Angstrom, A., The parameters of atmospheric turbidity, *Tellus*, *16*, 64–75, 1964.

Ansmann, A., D. Althausen, U. Wadinger, K. Franke, D. Mûller, F. Wagner, and J. Heintzenberg, Vertical profiling of the Indian aerosol plume with six-wavelength lidar during INDOEX: A first case study, *Geophys. Res. Lett.*, *27*(7), 963–966, 2000.

Berg, O. H., E. Swietlicki, and R. Krejci, Hygroscopic growth of aerosol particles in the marine boundary layer over the Pacific and Southern Oceans during the First Aerosol Characterization Experiment (ACE 1), *J. Geophys. Res.*, *103*, 16,535–16,545, 1998.

Browell, E. V., et al., Ozone and aerosol distributions and air mass characteristics over the South Atlantic Basin during the burning season, *J. Geophys. Res.*, *101*, 24,043–24,068, 1996.

Campbell, J. R., D. L. Hlavka, J. D. Spinhirne, R. Ferrare, and D. D. Turner, Automated aerosol retrieval algorithms for ARM micro pulse lidars, in *Preprints of Symposium on Lidar Atmospheric Monitoring*, pp. 71–74, American Meteorol. Soc., Boston, Mass., 2000.

Campbell, J. R., D. L. Hlavka, E. J. Welton, C. J. Flynn, D. D. Turner, J. D. Spinhirne, V. S. Scott, and I. H. Hwang, Full-time, eye-safe cloud and aerosol lidar observation at Atmospheric Radiation Measurement Program sites: Instruments and data processing, *J. Atmos. Oceanic Technol.*, *19*, 431–442, 2002.

Fernald, F. G., Analysis of atmospheric lidar observations: Some comments, *Appl. Opt.*, *23*, 652–653, 1984.

Ferrare, R. A., D. D. Turner, L. Heilman Brasseur, W. F. Feltz, O. Dubovik, and T. P. Tooman, Raman lidar measurements of the aerosol extinction-to-backscatter ratio over the Southern Great Plains, *J. Geophys. Res.*, *106*, 20,333–20,347, 2001.

Fuelberg, H. E., J. D. VanAusdall, E. V. Browell, and S. P. Longmore, Meteorological conditions associated with vertical distributions of aerosols off the west coast of Africa, *J. Geophys. Res.*, *101*, 24,105–24,115, 1996.

Garstang, M., P. D. Tyson, R. Swap, M. Edwards, P. Kallberg, and J. A. Lindesay, Horizontal and vertical transport of air over southern Africa, *J. Geophys. Res.*, *101*, 23,721–23,736, 1996.

Ginoux, P., M. Chin, I. Tegen, J. M. Prospero, B. Holben, O. Dubovik, and S.-J. Lin, Sources and distributions of dust aerosols simulated with the GOCART model, *J. Geophys. Res.*, *106*, 20,255–20,273, 2001.

Grousset, F. E., P. E. Biscaye, M. Revel, J. R. Petit, K. Pye, S. Joussaume, and J. Jouzel, Antarctic ice-core dust at 19 k.y.B.P.: Isotopic constraints on origins, *Earth Planet. Sci. Lett.*, *111*, 175–182, 1992.

Holben, B. N., et al., AERONET—A federated instrument network and data archive for aerosol characterization, *Remote Sens. Environ.*, *66*, 1–16, 1998.

Iriondo, M., Patagonian dust in Antarctica, *Quat. Int.*, *68*, 83–86, 2000.

Kent, G. S., C. R. Trepte, K. M. Skeens, and D. M. Winker, LITE and SAGE II measurements of aerosols in the southern hemisphere upper troposphere, *J. Geophys. Res.*, *103*, 19,111–19,127, 1998.

King, M. D., S. Platnick, C. C. Moeller, H. E. Revercomb, and S. A. Chu, Remote sensing of smoke, land and clouds from the NASA ER-2 during SAFARI 2000, *J. Geophys. Res.*, *108*, doi:10.1029/2002JD003207, in press, 2003.

Lassig, J. L., M. G. Cogliati, M. A. Bastanski, and C. Palese, Wind characteristics in Neuquen, North Patagonia, Argentina, *J. Wind Eng. Ind. Aerodyn.*, *79*(1–2), 183–199, 1999.

Legrand, D., A. Calahorrano, B. Guillier, L. Rivera, M. Ruiz, D. Villagomez, and H. Yepes, Stress tensor analysis of the 1998–1999 tectonic swarm of northern Quito related to the volcanic swarm of Guagua Pichincha volcano, Ecuador, *Tectonophysics*, *344*, 15–36, 2002.

Martins, J. V., P. V. Hobbs, R. E. Weiss, and P. Artaxo, Sphericity and morphology of smoke particles from biomass burning in Brazil, *J. Geophys. Res.*, *103*, 32,051–32,057, 1998.

McGill, M., D. L. Hlavka, W. D. Hart, E. J. Welton, and J. R. Campbell, Airborne lidar measurements of aerosol optical properties during SAFARI 2000, *J. Geophys. Res.*, *108*, doi:10.1029/2002JD002370, in press, 2003.

Nobre, C. A., L. F. Mattos, C. P. Dereczynski, T. A. Tarasova, and I. V. Trosnikov, Overview of atmospheric conditions during the Smoke, Clouds and Radiation-Brazil (SCAR-B) field experiment, *J. Geophys. Res.*, *103*, 31,809–31,820, 1998.

O'Dowd, C. D., J. A. Lowe, and M. H. Smith, Observations and modeling of aerosol growth in marine stratocumulus—Case study, *Atmos. Environ.*, *33*, 3053–3062, 1999.

Palm, S. P., W. D. Hart, D. L. Hlavka, E. J. Welton, and J. D. Spinhirne, *GLAS Atmospheric Data Products: Algorithm Theoretical Basis Document V4.1*, 111 pp., NASA Goddard Space Flight Cent., Greenbelt, Md., 2001.

Peppler, R. A., et al., ARM Southern Great Plains site observations of the smoke pall associated with the 1998 Central American fires, *Bull. Am. Meteorol. Soc.*, *81*, 2563–2591, 2000.

Piketh, S. J., H. J. Annegarn, and P. D. Tyson, Lower tropospheric aerosol loadings over South Africa: The relative contribution of Aeolian dust, industrial emissions, and biomass burning, *J. Geophys. Res.*, *104*, 1597–1607, 1999.

Powell, D. M., J. A. Reagan, M. A. Rubio, W. H. Erxleben, and J. D. Spinhirne, ACE-2 multiple angle micro-pulse lidar observations from Las Galletas, Tenerife, Canary Islands, *Tellus, Ser. B*, *52*, 651–660, 2000.

Reid, J. S., P. V. Hobbs, R. J. Ferek, D. R. Blake, J. V. Martins, M. R. Dunlap, and C. Liousse, Physical, chemical, and optical properties of regional hazes dominated by smoke in Brazil, *J. Geophys. Res.*, *103*, 32,059–32,080, 1998.

Remer, L. A., Y. J. Kaufman, B. N. Holben, The size distribution of ambient aerosol particles: Smoke versus Urban/Industrial aerosol, in *Biomass Burning and Global Change*, edited by J. Levine, pp. 519–530, Mass Inst. of Technol., Cambridge, Mass., 1996.

Russell, P. B., et al., Global to microscale evolution of the Pinatubo volcanic aerosol derived from diverse measurements and analyses, *J. Geophys. Res.*, *101*, 18,745–18,763, 1996.

Schmid, B., C. Matzler, A. Heimo, and N. Kampfer, Retrieval of the optical depth and particle size distribution of tropospheric and stratospheric aerosols by means of sun-photometry, *IEEE Trans. Geosci. Remote Sens.*, *35*, 172–182, 1997.

Schmid, B., et al., Coordinated airborne, spaceborne, and ground-based measurements of massive, thick aerosol layers during the dry season in Southern Africa, *J. Geophys. Res.*, *108*, doi:10.1029/2002JD002297, in press, 2003.

Smith, W. L., et al., The Chesapeake Lighthouse and Aircraft Measurements for Satellites (CLAMS) Experiment, paper presented at the 11th Satellite Meteorology and Oceanography Conference, Madison, Wisc., Am. Meteorol. Soc., Boston, Mass., Oct. 2001.

Spinhirne, J. D., Micro pulse lidar, *IEEE Trans. Geosci. Remote Sens.*, *31*, 48–55, 1993.

Spinhirne, J. D., J. A. Reagan, and B. A. Herman, Vertical distribution of aerosol extinction cross section and inference of aerosol imaginary index in the troposphere by lidar technique, *J. Appl. Meteorol.*, *19*, 426–438, 1980.

Spinhirne, J. D., J. A. R. Rall, and V. S. Scott, Compact eye safe lidar systems, *Rev. Laser Eng.*, *23*, 112–118, 1995.

Swap, R. J., M. Garstang, S. A. Macko, P. D. Tyson, W. Maenhaut, P. Artaxo, P. Kållberg, and R. Talbot, The long-range transport of southern African aerosols to the tropical south Atlantic, *J. Geophys. Res.*, *101*, 23,777–23,791, 1996.

Swap, R. J., et al., The Southern African Regional Science Initiative (SAFARI 2000) dry-season field campaign: An overview, *S. Afr. J. Sci.*, *98*, 125–130, 2002.

Takamura, T., Y. Sasano, and T. Hayasaka, Tropospheric aerosol optical properties derived from lidar, Sun photometer, and optical particle counter measurements, *Appl. Opt.*, *33*, 7132–7141, 1994.

Tanre, D., Y. J. Kaufman, B. N. Holben, B. Chatenet, A. Karnieli, F. Lavenu, L. Blarel, O. Dubovik, L. A. Remer, and A. Smirnov, Climatology of dust aerosol size distribution and optical properties derived from remotely sensed data in the solar spectrum, *J. Geophys. Res.*, *106*, 18,205–18,217, 2001.

Terblanche, D. E., M. P. Mittermaier, S. J. Piketh, R. T. Bruintjes, and R. P. Burger, The Aerosol Recirculation and Rainfall Experiment (ARREX): An initial study on aerosol-cloud interactions over South Africa, *S. Afr. J. Sci.*, *96*, 15–21, 2000.

Trentmann, J., M. O. Andreae, H.-F. Graf, P. V. Hobbs, R. D. Ottmar, and R. Trautmann, Simulation of a biomass-burning plume: Comparison of model results with observations, *J. Geophys. Res.*, *107*, 410–414, 2002.

Tyson, P. D., M. Garstang, and R. Swap, Large-scale recirculation of air over southern Africa, *J. Appl. Meteorol.*, *35*, 2218–2236, 1995.

Tyson, P. D., M. Garstang, R. Swap, P. Kallberg, and M. Edwards, An air transport climatology for subtropical southern Africa, *Int. J. Climatol.*, *16*, 265–291, 1996.

Voss, K. J., E. J. Welton, P. K. Quinn, J. Johnson, A. Thompson, and H. Gordon, Lidar measurements during Aerosols99, *J. Geophys. Res.*, *106*, 20,821–20,832, 2001.

Watson, I. M., and C. Oppenheimer, Photometric observations of Mt. Etna's different aerosol plumes, *Atmos. Environ.*, *35*, 3561–3572, 2001.

Welton, E. J., and J. R. Campbell, Micro-pulse lidar signals: Uncertainty analysis, *J. Atmos. Oceanic Technol.*, *19*, 2089–2094, 2002.

Welton, E. J., et al., Ground-based lidar measurements of aerosols during ACE-2: Instrument description, results and comparisons with other ground-based and airborne measurements, *Tellus, Ser. B*, *52*, 635–650, 2000.

Welton, E. J., J. R. Campbell, T. A. Berkoff, J. D. Spinhirne, and P. Ginoux, Initial results from the micro-pulse lidar network (MPL-Net), paper presented at the Fall Meeting of the American Geophysical Union, San Francisco, Calif., Dec. 2001a.

Welton, E. J., J. R. Campbell, J. D. Spinhirne, and V. S. Scott, Global monitoring of clouds and aerosols using a network of micro-pulse lidar systems, *Proc. Int. Soc. Opt. Eng.*, *4153*, 151–158, 2001b.

Welton, E. J., K. J. Voss, P. K. Quinn, P. J. Flatau, K. Markowicz, J. R. Campbell, J. D. Spinhirne, H. R. Gordon, and J. E. Johnson, Measurements of aerosol vertical profiles and optical properties during INDOEX 1999 using micropulse lidars, *J. Geophys. Res.*, *107*, 8019, doi:10.1029/2000JD000038, 2002.

M. Barenbrug and S. J. Piketh, University of Witwatersrand, East Campus, Private Bag X3, WITS 2050, South Africa. (margie@crg.bpb.wits.ac.za; stuart@crg.bpb.wits.ac.za)

J. R. Campbell, J. D. Spinhirne, and E. J. Welton, NASA Goddard Space Flight Center, Code 912, Greenbelt, MD 20771, USA. (campbell@virl.gsfc.nasa.gov; jspin@virl.gsfc.nasa.gov; Ellsworth.J.Welton@nasa.gov)

B. Holben, NASA Goddard Space Flight Center, Code 923, Greenbelt, MD 20771, USA. (brent@aeronet.gsfc.nasa.gov)

Q. Ji and S.-C. Tsay, NASA Goddard Space Flight Center, Code 913, Greenbelt, MD 20771, USA. (ji@climate.gsfc.nasa.gov; tsay@climate.gsfc.nasa.gov)